Design and Implementation of End-Pumped Neodymium: YAG Lasers

A Thesis
Submitted to the Department of Electrical and Electronics Engineering
and the Institute of Engineering and Sciences
of Bilkent University
In Partial Fulfillment of the Requirements
For the Degree of
Master of Science

By
Salih Uğur

February 1996

TA
1705
.U48
1996

DESIGN AND IMPLEMENTATION OF END-PUMPED NEODYMIUM:YAG LASERS

A THESIS

SUBMITTED TO THE DEPARTMENT OF ELECTRICAL AND

ELECTRONICS ENGINEERING

AND THE INSTITUTE OF ENGINEERING AND SCIENCES

OF BİLKENT UNIVERSITY

IN PARTIAL FULFILLMENT OF THE REQUIREMENTS

FOR THE DEGREE OF

MASTER OF SCIENCE

By

Salih Uğur

Salih Uğur
tarafından [illegible]

February 1996

TA
1705
.U48
1936

B.1,33676

I certify that I have read this thesis and that in my opinion it is fully adequate, in scope and in quality, as a thesis for the degree of Master of Science.

Assist. Prof. Dr. Orhan Aytür (Supervisor)

I certify that I have read this thesis and that in my opinion it is fully adequate, in scope and in quality, as a thesis for the degree of Master of Science.

Prof. Dr. Ayhan Altıntaş

I certify that I have read this thesis and that in my opinion it is fully adequate, in scope and in quality, as a thesis for the degree of Master of Science.

Assist. Prof. Dr. Ekmel Özbay

Approved for the Institute of Engineering and Sciences:

Prof. Dr. Mehmet Baray
Director of the Institute of Engineering and Sciences

ABSTRACT

DESIGN AND IMPLEMENTATION OF END-PUMPED NEODYMIUM:YAG LASERS

Salih Uğur
M.S. in Electrical and Electronics Engineering
Supervisor: Assist. Prof. Dr. Orhan Aytür
February 1996

In this study, we implemented end-pumped Fabry-Perot and ring Neodymium:YAG lasers operating at 1064 nm. Intracavity frequency doubling of these lasers to 532 nm was also achieved. A 4 W diode laser was used as a pump source. Diode light was transferred to the Nd:YAG crystal via various optics. 2.5 W pump power was incident on the Nd:YAG crystal. Various Fabry-Perot resonator configurations were implemented and evaluated. A maximum output power of 780 mW was obtained. This corresponds to 31% optical conversion efficiency. A strong relationship between the laser performance and the radius of the laser mode was observed. It is also noted that the wavelength of the diode light is a very important parameter for laser performance. In addition to Fabry-Perot lasers, a ring laser was implemented, yielding a maximum output power of 230 mW. With these two types of lasers, intracavity frequency doubling experiments were carried out using a KTP crystal. 165 mW and 85 mW maximum output powers at 532 nm were obtained from intracavity frequency doubled Fabry-Perot and ring lasers, respectively.

Keywords : lasers, Nd:YAG, diode lasers, diode-pumped, end-pumped, frequency doubling, second harmonic generation.

ÖZET

ARKADAN-POMPALANMIŞ NEODİMYUM:YAG LAZERLERİN TASARIMI VE YAPIMI

Salih Uğur
Elektrik ve Elektronik Mühendisliği Bölümü Yüksek Lisans
Tez yöneticisi: Yar. Doç. Dr. Orhan Aytür
Şubat 1996

Bu çalışmada 1064 nm'de çalışan arkadan pompalanmış Fabry-Perot ve halka Neodimyum:YAG lazerler yapılmıştır. Bu lazerlerle resonatör-içi frekans katlaması yoluyla 532 nm'de çıkış da elde edilmiştir. Pompa kaynağı olarak 4 W'lık bir diyot lazer kullanılmıştır. Diyot ışığı çeşitli optikler yoluyla Nd:YAG'a iletilmiştir. Nd:YAG'a ulaşan pompa gücü 2.5 W'dır. Çeşitli Fabry-Perot resonatör geometrileri yapılmış ve değerlendirilmiştir. Elde edilen en yüksek güç 780 mW olmuştur. Bu, %31'lik optik dönüşüm verimine denk gelmektedir. Lazerin performansı ile lazer modu yarıçapı arasında güçlü bir bağlantı gözlemlenmiştir. Ayrıca, diyot lazer dalgaboyunun lazerin performansı için çok önemli bir değişken olduğu kaydedilmiştir. Fabry-Perot lazerlerinden başka, en yüksek gücü 230 mW olan bir halka lazeri de gerçekleştirilmiştir. Bu iki çeşit lazerle, KTP kristali kullanılarak resonatör-içi frekans katlaması deneyleri yapılmıştır. Bu resonatör-içi frekans katlamalı Fabry-Perot ve halka lazerlerinden 532 nm dagaboyunda sırasıyla 165 mW ve 85 mW güç elde edilmiştir.

Anahtar Kelimeler: lazerler, Nd:YAG, diyot lazerler, diyotla-pompalanmış, arkadan-pompalanmış, frekans katlaması, ikinci harmonik üretimi.

ACKNOWLEDGMENTS

I would like to thank Dr. Orhan Aytür for his supervision, guidance, suggestions, and encouragement through the development of this thesis.

TABLE OF CONTENTS

LIST OF FIGURES

LIST OF TABLES

Chapter 1

INTRODUCTION

Lasers are devices that generate coherent light beams. A coherent beam has a fixed phase over the cross-section of the beam and a very narrow bandwidth. The frequency range of lasers extends from microwaves to soft-x-rays. Because of their unique properties, lasers find applications in many diverse areas of science and technology. Amongst these are optical communications, military systems, remote sensing, medicine, and optical data storage.

The first successful laser was built in 1960 [1]. This was a flash-lamp-pumped ruby laser. Many different types of lasers were developed soon after. Among these, solid-state lasers are unique for their higher efficiency, design simplicity, and compactness.

Solid-state lasers are mostly optically pumped. Early solid-state lasers were pumped with flashlamps. The advent of semiconductor lasers brought about another possible pump source. Nowadays, both of these pump sources, flashlamps and diode lasers, are used to pump solid-state lasers. Flashlamp-pumped lasers have greater output powers, but have lower efficiencies due to the broad spectral output of flashlamps. Diode-pumped lasers offer higher efficiencies and much better stability compared to flashlamp-pumped lasers. The output powers of diode-pumped lasers are also increasing steadily due to rapid advances in diode laser technology and innovative laser designs.

In diode-pumped lasers, there are two alternatives for the pumping geometry. One is side-pumping in which the diode or diodes are placed around the laser material. In this geometry, pump light is absorbed starting from the outer edges to the inner parts of the laser material. The advantage of side-pumped lasers is their higher output powers, since the number of diode lasers that are

placed around the gain medium can be increased easily. The other geometry is end-pumping where the diode is positioned towards one of the faces of the laser material. The pump beam from the diode is collinear with the optical resonator, hence the overlap between the pumped volume and fundamental laser mode can be very high. Moreover, the laser material can be made longer than the absorption length of the pump light, so that a large fraction of the pump beam can be absorbed. These properties lead to higher efficiencies and better beam qualities.

Neodymium-doped yttrium aluminum garnet (Nd:YAG) is a widely used solid-state laser material because of its favorable optical and physical properties. It has several possible lasing wavelengths, the strongest of which is at 1064 nm. Nd:YAG has absorption bands near 810 nm where AlGaAs diode lasers operate. This makes Nd:YAG a natural choice for diode-pumping.

Lasers are constructed by placing a gain medium inside an optical resonator. Optical resonators can be classified into two groups, Fabry-Perot resonators and ring resonators. Fabry-Perot resonators are implemented by placing two mirrors in parallel. A standing wave pattern is set up inside Fabry-Perot resonators. Standing waves inside the gain medium create an effect called spatial hole burning, which prevents single longitudinal mode operation of the laser. Spatial hole burning can be eliminated using ring resonators. A ring laser that is operated unidirectionally, with the help of an isolator inside the resonator, will have no standing waves, and therefore no spatial hole burning. The disadvantage of ring lasers is that the gain medium is traversed only once in one round trip.

The output wavelength diversity of lasers are limited to the number of possible atomic transitions of laser materials. To extend the wavelength range of lasers, nonlinear optical properties of various materials are utilized. Frequency doubling is one of the nonlinear optical processes with which new frequencies can be generated. Frequency doubling (second harmonic generation) can be achieved by passing the laser beam through a suitable nonlinear material. Alternatively, the nonlinear material may be placed inside the laser resonator to take advantage of the larger intensities there. This method is called intracavity frequency doubling. There are many crystals that can be used for second harmonic generation. The one especially suitable for using with Nd:YAG lasers is Potassium Titanyl Phosphate (KTP). A portion of the light from Nd:YAG at 1064 nm is converted to light at 532 nm as it passes through an appropriately oriented KTP crystal.

In this thesis, we designed and implemented Nd:YAG lasers. As a pump source, we used a diode laser with 4 W output power. The highly divergent light of the diode was collimated with a high numerical aperture compound lens. After that, a cylindrical lens was used to correct the astigmatism of the beam. The pump light was focused to a spot of 600 μm by 100 μm using a spherical lens. The focused pump beam was used to end-pump a 1 cm long Nd:YAG crystal. 98% of the incident pump power is absorbed in the crystal. The faces of the Nd:YAG crystal were cut at Brewster's angle to reduce reflection losses and to induce polarized output light.

We implemented different Fabry-Perot lasers by changing the input coupler mirror radius of curvature, the output coupler transmittance, and the resonator length. Changing the input coupler radius and the resonator length affects the laser mode size. Hence, we observed the performance of the laser at different mode sizes. By implementing lasers with different output couplers, we tried to determine the optimum output coupler transmittance.

A ring laser was also implemented which operated bidirectionally due to the lack of an isolator.

Intracavity frequency doubling of the laser light was achieved with Fabry-Perot and ring lasers. A KTP crystal was used for this purpose.

Chapter 2 presents the theoretical background to explain basic laser properties and design criteria. The pumping scheme of our laser is described in Chapter 3. In Chapter 4, the results and analyses of Fabry-Perot laser experiments are presented. In Chapter 5, the ring laser design is explained. Intracavity frequency doubling experiments are described in Chapter 6. Finally, remarks and conclusions are provided in Chapter 7.

Chapter 2

THEORETICAL BACKGROUND

This chapter gives the basic theory that underlies our experiments. First, a simple theory is given for continuous wave (cw) lasers. Then, the diode laser end-pumping scheme is described. Explanations of ring lasers and frequency doubling are given next. At the end, a brief history of experimental work done in this field is given.

2.1 Basic laser theory

A laser is an oscillator at optical frequencies. As in electronic oscillators, there are two essential parts of a typical laser (see Figure 2.1):

- Amplification.
- Positive feedback.

Amplification is achieved through a gain medium which is a material consisting of an appropriate collection of atoms, molecules, ions or electrons. Optical gain is obtained by exciting the material system into higher quantum mechanical energy levels to create a population inversion. This excitation operation is called the pumping process.

The mirrors placed around the gain medium in a laser supply the feedback. By properly aligning these mirrors, the beam inside the resonator can

be bounced back and forth between them. The beam is amplified at every pass through the gain medium. If the net amplification exceeds the total losses (due to mirrors, scattering, etc...), then laser oscillation will build up. The output beam can be coupled from this oscillation via a partially transmitting mirror (output coupler).

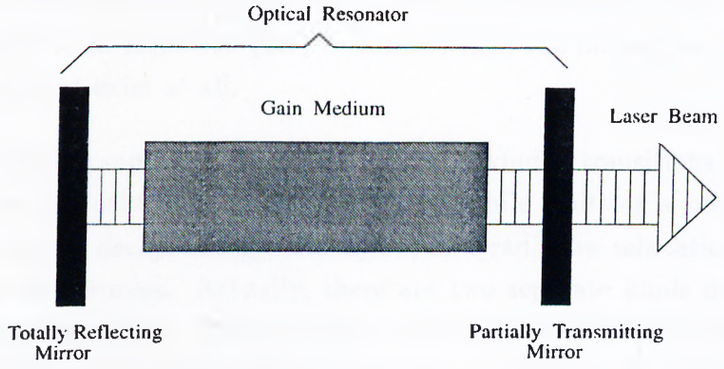

Figure 2.1: A generic laser.

2.1.1 Absorption and emission

In the laser gain medium, the electronic charge distribution of atoms, molecules or ions creates energy levels. Absorption or emission of a photon is the result of the upward or downward transition (respectively) of an atom between two of its energy levels. A simplified two level energy diagram is shown in Figure 2.2.

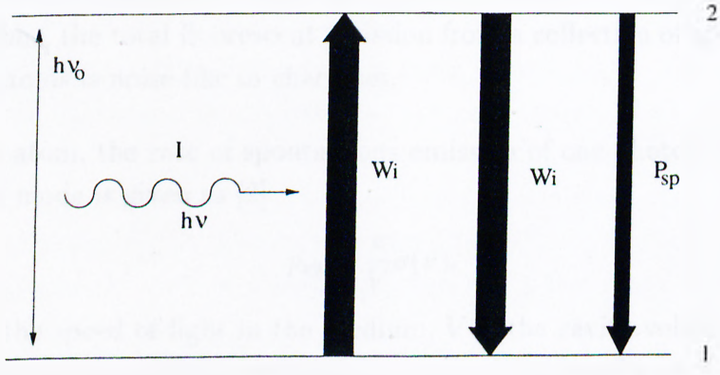

Figure 2.2: Simplified two-level energy level diagram.

There are three different types of interactions between the atom and the photon. For any of interactions to occur, the energy of the photon should be

close to the energy difference between the levels of the atom

$$E_2 - E_1 = h\nu_0 \simeq h\nu \tag{2.1}$$

where $h = 6.63 \times 10^{-34}$ J-s is Planck's constant, ν is the frequency of the photon, and $E_2 - E_1$ is the energy difference between the atomic energy levels [2]. In other words, the light field must be in resonance with the atomic transition. If the condition in Equation (2.1) is not satisfied, the interaction will be very weak or will not exist at all.

First, there is spontaneous emission. In this kind of transitions, upper level atoms spontaneously drop to the lower level while emitting a photon. Fluorescence, energy decay, energy relaxation, and radiative relaxation are other names for this process. Actually, there are two separate kinds of downward spontaneous transitions. One is radiative transitions which we called spontaneous emission. The other one is nonradiative transitions where the transition energy is released not by radiating electromagnetic radiation, but by setting up mechanical vibrations of the surrounding crystal lattice. When atoms are placed in an upper level, they decay downward by a combination of radiative and nonradiative decay processes. The relative rates of these transitions is different for every atomic transition and depends on the immediate surroundings of the atoms.

In spontaneous emission, each individual atom radiates independently, with a phase angle that is independent of all the other radiating atoms. Photons can be characterized by a sum of orthogonal electromagnetic modes [2]. The spontaneous emission is also independent of the number of photons that may already exist in these modes and the emitted photon can be coupled in any modes. Thus, the total fluorescent emission from a collection of spontaneously emitting atoms is noise-like in character.

For an atom, the rate of spontaneous emission of one photon into a single prescribed mode is given as [2]

$$p_{sp} = \frac{c}{V}\sigma(\nu). \tag{2.2}$$

Here, c is the speed of light in the medium, V is the cavity volume, and $\sigma(\nu)$ is the transition cross section which is a narrow function of ν centered around the atomic resonance frequency. In this equation, the atom is assumed to be inside a cavity of volume V, for simplicity. However, this assumption does not pose a loss of generality [2]. The transition cross section for a specific transition can be calculated using Schrödinger's equation, but the calculations are very complicated. Therefore, $\sigma(\nu)$ is usually determined experimentally.

Experimentally measurable quantities that give the transition cross section are the spontaneous fluorescence lifetime t_{sp} and the lineshape function $g(\nu)$. The spontaneous fluorescence lifetime is defined as the decay time of excited atoms spontaneously falling to lower level by emitting a photon. The relation between the transition cross section and the lineshape function is given by

$$\sigma(\nu) = Sg(\nu) \tag{2.3}$$

where

$$S = \int_0^\infty \sigma(\nu)d\nu \tag{2.4}$$

and it is called the transition strength. The transition strength is obtained from the spontaneous fluorescence lifetime. The relation between them is given by

$$S = \frac{\lambda^2}{8\pi t_{sp}}. \tag{2.5}$$

Here, λ is the wavelength. Equation (2.2) gives probability of emitting a photon into one mode, but the spontaneous emission can be into any mode. For an atom, the rate of spontaneous emission of one photon into any mode is given by

$$P_{sp} = \frac{1}{t_{sp}} = \frac{8\pi S}{\lambda^2} \tag{2.6}$$

which is obtained by integrating Equation (2.2) over all possible modes.

When a light field near resonance with a pair of energy levels is propagating through the medium, two types of stimulated processes occur, namely stimulated emission and stimulated absorption. Stimulated absorption results in the loss of a photon from the light field. The energy of the photon is transfered to the medium by increasing the energy of an atom from a lower energy level to a higher one. Stimulated emission results in an increase in the number of photons (light intensity) when an atom drops from a higher energy level to a lower one. In this case, the emitted photons have exactly the same characteristics (frequency, direction, polarization, etc...) with the original (stimulating) photons. This is the key process behind lasers. Both of these stimulated processes have the same rate. The rate of emitting a photon (if the atom is in the upper level) and the rate of absorbing a photon (if the atom is in the upper level) are both given by

$$W_i = \phi\sigma(\nu) \tag{2.7}$$

where $\phi = I/h\nu$ is the mean photon flux density (photons per second per unit area) and I is the optical intensity.

If there are N_1 atoms (per unit volume) at the lower level in the medium, then the number of absorbed photons is $N_1 W_i$. Similarly, if there are N_2 atoms

at the upper level, then the number of emitted photons is $N_2 W_i$. Therefore, the net number of gained photons will be NW_i, where N is the population difference ($N = N_2 - N_1$). Thus, for a beam of photons propagating along the z direction, the incremental number of photons per unit area per unit time can be written as [2]

$$d\phi = NW_i dz. \tag{2.8}$$

Equation (2.8) can be written in the form of a differential equation

$$\frac{d\phi(z)}{dz} = \gamma(\nu)\phi(z) \tag{2.9}$$

where $\gamma(\nu)$ is called the gain coefficient

$$\gamma(\nu) = N\sigma(\nu). \tag{2.10}$$

The solution of Equation (2.9) is

$$\phi(z) = \phi(0)\exp[\gamma(\nu)z]. \tag{2.11}$$

This is an exponential function of $\gamma(\nu)z$ which is directly proportional to the population difference N. If $N_2 > N_1$ (N is positive) the medium acts as an amplifier. If $N_2 < N_1$ (N is negative) the medium acts as an absorber. In thermal equilibrium. N_2 is always less than N_1, therefore N is always negative [3]. As a result, the medium acts as an absorber in thermal equilibrium.

2.1.2 Population inversion

To achieve amplification of light passing through the medium, the population of the higher energy level should be larger than that of the lower level (see Figure 2.3). An external source of energy is required to populate the specified energy level so as to create a population inversion. This energy is provided by an external pumping mechanism.

The mechanism of pumping requires the use of additional energy levels other than those directly involved in the amplification process. The population inversion between desired levels is obtained indirectly by exciting the atoms into other energy levels. The pumping and laser processes in real laser systems typically involve a large number of energy levels, with complex excitation and cascaded relaxation processes among all these levels. However, almost all lasers can be modeled as systems with three or four energy levels and some important insights can be gained by analyzing these simplified three or four-level energy diagrams. Since Nd:YAG is a four-level laser system, we

present the energy diagram (see Figure 2.4 [2]) and some relations of four-level lasers here. Lifetimes, which are inverses of transition rates, of corresponding energy levels are shown with τ in the figure.

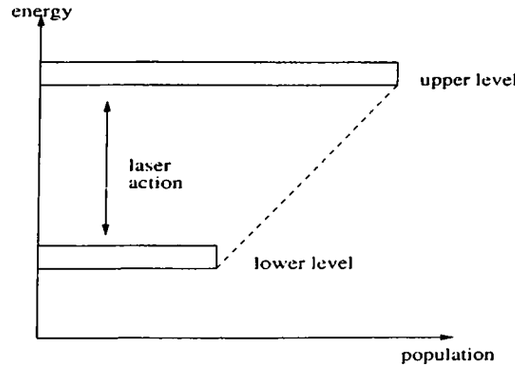

Figure 2.3: Population inversion between two energy levels.

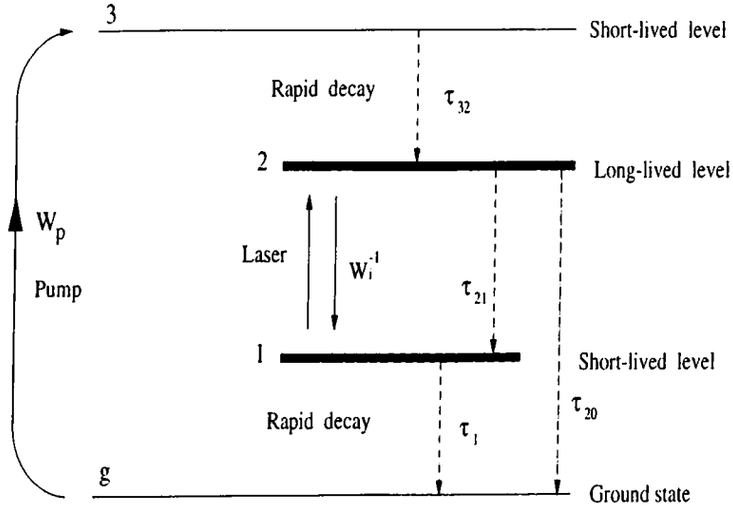

Figure 2.4: Four-level system.

In four-level systems, the pump transition is from the ground state (level g) to an absorption band (level 3). The 3→2 transition has a short lifetime, so that the atoms excited to level 3 will proceed rapidly to level 2. There is negligible population in level 3 through the laser process ($N_3 \simeq 0$). Level 2 has a long lifetime and therefore it accumulates population. The laser transition occurs between the level 2 and the level 1. Level 1 is a short-lived level and sustains little population ($N_1 \simeq 0$). From here the atom undergoes a rapid transition to the ground level. The population difference in an optically pumped four-level

laser system can be written as [2]

$$N = \frac{W_p N_a \tau_2 (1 - \tau_1/\tau_{21})}{1 + W_i(\tau_2 + \tau_1(1 - \tau_2/\tau_{21})) + W_p(\tau_2(1 - \tau_1/\tau_{21}))}. \tag{2.12}$$

Here, W_p is the pumping rate, N_a is the total atomic density of the material, and τ_2 is the overall lifetime of the level 2 ($\tau_2^{-1} = \tau_{21}^{-1} + \tau_{20}^{-1}$). Usually, four-level systems with $\tau_{21} \gg \tau_2 \gg \tau_1$ and $\tau_2 \simeq t_{sp}$ are preferred as a gain medium in real lasers because of their higher obtainable population differences, so the Equation (2.12) can be simplified to

$$N = \frac{N_0}{1 + \tau_s W_i} \tag{2.13}$$

where

$$N_0 = \frac{t_{sp} N_a W_p}{1 + t_{sp} W_p} \tag{2.14}$$

and

$$\tau_s = \frac{t_{sp}}{1 + t_{sp} W_p}. \tag{2.15}$$

Here N_0 is called the steady-state population difference in the absence of radiation, and τ_s is called the saturation time constant. As clearly seen from Equation (2.13), even in the case of very weak pumping, population inversion is achieved.

2.1.3 The optical resonator

In a laser, optical feedback is obtained by placing the gain medium in an optical resonator. Optical resonators give rise to modes of the laser. There are two types of resonator modes; longitudinal modes which differ from one another by their oscillation frequency and transverse modes which differ from one another in their field distribution at a plane perpendicular to the direction of propagation. The beam divergence, beam diameter, and transverse energy distribution of the laser beam are determined by transverse modes, while linewidth and coherence length are determined primarily by longitudinal modes.

In an optical resonator, only light waves whose amplitude and phases reproduce themselves after one round trip through the resonator can be sustained. These waves comprise the modes of the resonator. Transverse modes are classified by the designation TEM_{mn} for Cartesian coordinates. The integers m and n represent the number of zeros in the intensity pattern in the vertical and horizontal directions, respectively. The lowest order mode is TEM_{00} whose intensity profile is a Gaussian distribution. The resonator may build up Gaussian

beams (fundamental mode) or Laguerre-Gaussian beams (higher order modes) inside a laser. Fundamental mode Gaussian beams have better beam properties (small divergence angle, no zeros in the intensity pattern, etc...) than higher order mode beams, so it is generally preferred to operate a laser in TEM_{00} mode. Algebraic methods can be applied to find the parameters of a Gaussian beam for a specific resonator [4], [5]. $ABCD$ matrix methods can also be used [2], [3]. The general characteristics of Gaussian beams are given in Appendix A.

Longitudinal modes of the resonator are waves at discrete frequencies

$$\nu_q = q\frac{c}{2d} \qquad q = 1, 2, ... \tag{2.16}$$

where q is the mode number and d is the length of the resonator. Laser oscillation can build up only at these frequencies because the round trip phase difference is an integer multiple of 2π for these frequencies. The separation of the longitudinal modes in a laser cavity is given by

$$\nu_f = \frac{c}{2d}. \tag{2.17}$$

The optical resonator also contributes to the losses in the laser system. In one round trip through the laser, the beam experiences several losses and its magnitude decreases to $R_1 R_2 \exp(-\alpha_s d)$ times the original magnitude (for a two mirror resonator). Here R_1 and R_2 are the reflectances of the mirrors, d is the resonator length and α_s is the distributed loss caused by absorption and scattering of light in the medium. The overall loss in one round trip can be written as a total effective distributed loss coefficient α_r by [2]

$$\exp(-2\alpha_r d) = R_1 R_2 \exp(-2\alpha_s d) \tag{2.18}$$

where

$$\alpha_r = \alpha_s + \alpha_{m1} + \alpha_{m2} \tag{2.19}$$

$$\alpha_{m1} = \frac{1}{2d} \ln \frac{1}{R_1} \tag{2.20}$$

$$\alpha_{m2} = \frac{1}{2d} \ln \frac{1}{R_2} \tag{2.21}$$

α_{m1} and α_{m2} are the contributions of the mirrors 1 and 2 respectively to the total loss coefficient.

2.1.4 Laser output power

In a laser amplifier, the gain coefficient of the gain medium is dependent on the photon-flux density that is to be amplified [2]

$$\gamma(\nu) = \frac{\gamma_0(\nu)}{1 + \phi/\phi_s(\nu)}. \tag{2.22}$$

As the photon-flux density increases, the amplifier enters a region of nonlinear operation. It saturates and its gain decreases. In this equation, $\phi_s(\nu)$ is the saturation photon-flux density and $\gamma_0(\nu)$ is the small signal gain coefficient. Their relation to known quantities are given by

$$\gamma_0(\nu) = N_0\sigma(\nu) \tag{2.23}$$

$$\phi_s(\nu) = [\tau_s\sigma(\nu)]^{-1}. \tag{2.24}$$

In these equations, N_0 increases with increasing pumping rate and τ_s is related to the decay times of energy levels.

In order for the laser to operate, its small-signal gain coefficient should be greater than the loss coefficient;

$$\gamma_0(\nu) > \alpha_r. \tag{2.25}$$

From this equation, the minimum population difference, namely the threshold population difference, that will allow lasing is obtained as

$$N_t = \frac{\alpha_r}{\sigma(\nu)}. \tag{2.26}$$

Also, Equation (2.25) can be written in terms of population densities as

$$N_0 > N_t. \tag{2.27}$$

When a laser is pumped above the threshold ($N_0 > N_t$), an oscillation will begin from spontaneously emitted photons. The photon flux density inside the laser cavity increases. This increase in the photon flux density causes the gain coefficient to saturate and decrease according to the Equation (2.22). When the saturated gain coefficient becomes equal to the loss coefficient ($\gamma = \alpha_r$ or $N = N_t$), steady-state condition is reached, and the photon flux density inside the laser is given by

$$\phi = \phi_s(\nu)\left[\frac{\gamma_0(\nu)}{\alpha_r} - 1\right] \tag{2.28}$$

or in a different form

$$\phi = \phi_s(\nu)\left[\frac{N_0}{N_t} - 1\right]. \tag{2.29}$$

Some portion of this photon flux density is coupled as an output through the output coupler with transmittance $T = 1 - R$. This output flux is given by

$$\phi_o = \frac{T\phi}{2}. \tag{2.30}$$

The intensity of the laser output and the output power are given by

$$I_o = \frac{h\nu T\phi}{2} \tag{2.31}$$

and

$$P_o = I_o A \tag{2.32}$$

where A is the cross-sectional area of the laser beam.

From Equations (2.31) and (2.32), we obtain the output power as a function of the output coupler transmittance. The output is zero for T=0, and also for large transmissions (the loss coefficient becomes larger than the small signal gain coefficient). For a specific value of transmittance, the output becomes maximum. To find this optimum output coupler transmittance, first the output photon flux density is written as a function of mirror transmittance in its open form

$$\phi_o = \frac{1}{2}\phi_s T\left[\frac{g_0}{L - ln(1-T)} - 1\right] \tag{2.33}$$

where

$$g_0 = 2\gamma_0(\nu)d \tag{2.34}$$

and

$$L = 2(\alpha_s + \alpha_{m2})d. \tag{2.35}$$

Here d is the resonator length, m_1 is the output coupler, and L corresponds to useless losses of the resonator. For maximum output power, the optimum transmittance can be found by setting the derivative of ϕ_o with respect to T equal to zero. For $T \ll 1$ the optimum transmittance can be reduced to a simple equation

$$T_{\text{opt}} = \sqrt{g_0 L} - L \tag{2.36}$$

and for this value of transmittance, the output photon flux density is given by

$$\phi_{\text{opt}} = \frac{1}{2}g_0\phi_s\left(1 - \sqrt{L/g_0}\right)^2. \tag{2.37}$$

The resonator useless losses L and the round trip gain g_0 should be known in order to find the optimum output coupler reflectance. Following a method first proposed by Findlay [6] these two parameters can be determined experimentally. In this method, output mirrors with different reflectivities are used

and threshold power for lasing for each mirror is measured. These two are related to each other by the following formula

$$-\ln R = 2KP_{\mathrm{TH}} - L \tag{2.38}$$

where R is the reflectivity of the output coupler, P_{TH} is the input power at threshold and K is called the conversion factor which combines all the efficiency factors. Extrapolation of the straight line plot of $-\ln R$ versus P_{TH}, at $P_{\mathrm{TH}} = 0$. yields the round trip loss L (see Figure 2.5). The slope of the straight line is $2K$ and g_0 can be calculated from $g_0 = 2KP_{\mathrm{in}}$ [7].

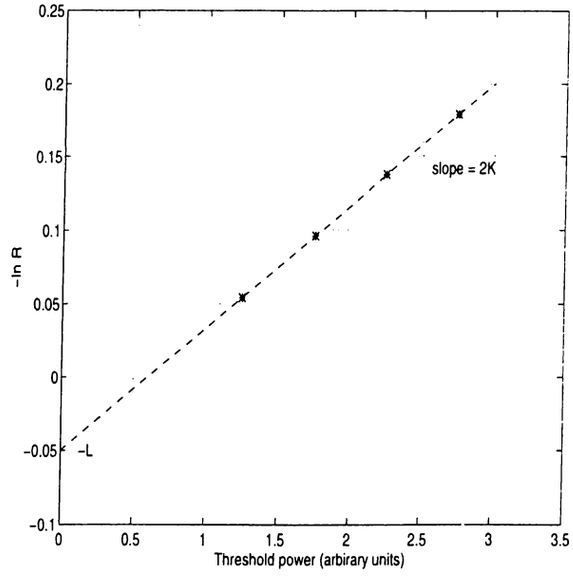

Figure 2.5: Determining the useless losses and the round trip gain coefficient from a -ln(R) versus threshold power graph for a typical laser.

Here we have to mention about K and efficiencies in more detail. The relation between K and efficiencies is given by

$$K = \eta_a \eta_u \eta_B / A\phi_s. \tag{2.39}$$

In Equation (2.39), A is the area of the beam and ϕ_s is the saturation photon-flux density defined earlier. Definitions of efficiencies are given below.

- η_a : absorption efficiency, is the ratio of the absorbed pump energy to the incident pump energy.
- η_u : upper state efficiency, is the ratio of the energy emitted at the laser transition to the energy absorbed at the pump bands.

- η_B : beam overlap efficiency, is the normalized overlap integral between the pump and laser modes.

We also define some other efficiencies necessary to evaluate laser performance.

- Slope efficiency : ratio of the output power increase to the input power increase.
- Optical conversion efficiency : ratio of the output power to the input optical power to the gain medium.
- Wall-plug efficiency : ratio of the output power to the electrical input power.

2.2 End pumping

To create population inversion inside the laser material, a pump source is required. In general, solid-state lasers are pumped by optical sources. The light from this sources is absorbed by the laser material. The absorbed energy creates population inversion by exciting the atoms of the gain medium into higher energy levels.

Optical pump sources can be classified into lamps (discharge and filament) and semiconductor sources (laser diodes and LED's). The radiation from a lamp has very broad spectral bandwidth. However, only a portion of it which falls in to the absorption spectrum of the gain medium is utilized. Therefore, the pumping efficiency of the lamp-pumped systems is very low. Also, the lamp-pumped systems need extensive cooling and this is the source of serious noise in the overall laser system. The advantage of using lamps as a pump source is that higher average powers are obtained from lamp-pumped systems, because lamps could supply very large powers (in the order of kW).

Recently, interest in diode laser-pumped systems has increased due to their advantages over lamp-pumped systems. Diode lasers have much narrower linewidths compared to lamps. Hence, the match between the emission spectra of the diode and the absorption spectra of the gain medium is better than lamp-pumped systems. Therefore, greater proportions of the radiation emitted from diode is absorbed by the laser material. This leads to increase of the

overall system efficiency. Also, the small size of diodes provides the design of more compact lasers that are entirely made of solid-state devices. Moreover, diode lifetimes are longer compared to lifetimes of lamps. The main disadvantage of diode-pumped lasers compared to lamp-pumped systems is their low output powers. However, scaling of diode-pumped systems to higher power levels appears feasible due to the rapid advances in diode laser technology and innovative pumping geometries.

There are two types of pumping schemes to couple the light of the diode laser to the gain medium (see Figure 2.6). These are side-pumped and end-pumped configurations. In side-pumped lasers, diodes are placed around the laser rod. As a result, the number of diodes can be increased to achieve desired power levels.

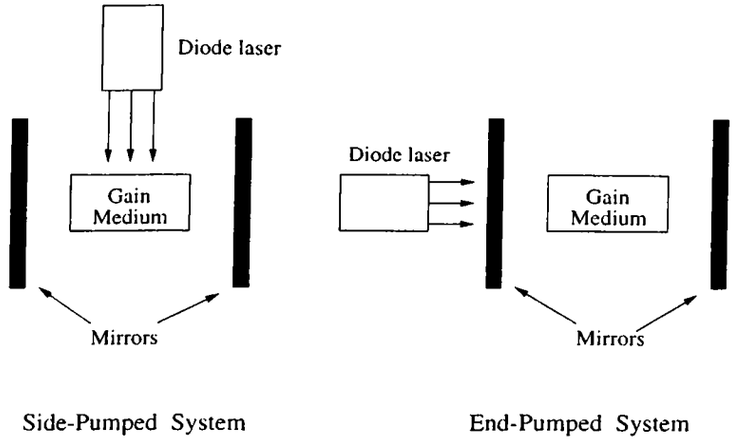

Figure 2.6: Side-pumped (left) and end-pumped (right) lasers.

The diode is positioned near the face of the gain medium in end-pumped lasers. The direction of the beam of the diode is collinear with the axis of the laser rod. The difficulty in end-pumped systems is in scaling to higher power levels, because only a small number of diodes can be placed at the ends of the gain medium compared to the sides.

The important advantages of end-pumped lasers over side-pumped lasers are high efficiency and good beam quality. The pump beam is absorbed along the laser rod in end-pumped systems while it is absorbed starting from the circumference through the center of the rod in side-pumped lasers. Therefore, a larger fraction of the pumped volume overlaps with the laser mode in end-pumped systems. This leads to a higher efficiency for end-pumped lasers. Also, the pumping of only the desired laser mode (usually TEM_{00}) can be achieved in end-pumped systems. Hence, lasers with good beam quality can be designed

without much effort.

For efficient pumping of a TEM_{00} mode end-pumped laser, two requirements must be met [8]. First, the gain medium must be long enough to absorb a large fraction of the pump light. Second, the radius of the pump beam must be less than or equal to the fundamental mode radius (see Figure 2.7). There is a number of reports showing the dependence of laser performance on the ratio of the pump beam and the resonator mode sizes [8]-[16]. In these papers, the performance of a laser is analyzed theoretically in terms of the mode sizes of the pump and laser beams. The analytical results are also supported experimentally. As a result, for good laser properties (low threshold and high gain), it is desirable to have small spot sizes, both for pump and laser modes. For a specific example, Hall [13], determined threshold power and efficiency for two cases. First, pump size is varied while the laser mode size is held constant; second the laser mode size is varied while the pump size is held constant. The best performance is obtained when the laser mode size approximately equals to the pump size for these two cases. It is also demonstrated that the size of the pump distribution is more important than the shape of that distribution as long as the pump energy is contained well within the laser mode.

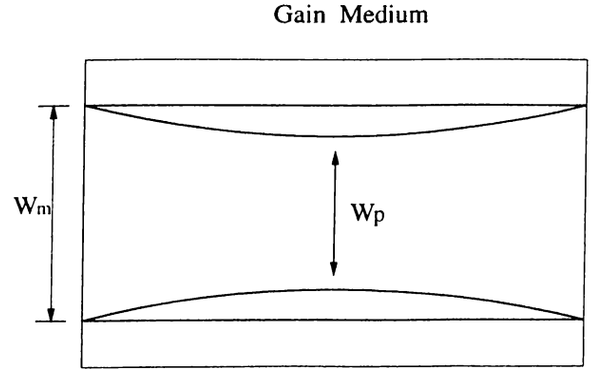

Figure 2.7: Mode sizes of pump beam (W_p) and laser beam (W_m) inside the gain medium.

2.3 Ring lasers

Figure 2.8 shows a typical ring laser. The beam follows a closed path like a ring inside the resonator.

In standing wave resonators, two waves traveling in opposite directions exist simultaneously in the laser medium. Interference between these two waves

produces a standing wave pattern in the optical intensity. This intensity variation leads to spatial variations in the amount of saturation along the laser medium. This phenomena is known as spatial hole burning. The unsaturated regions inside the gain medium can induce other longitudinal modes and thus prevent single longitudinal mode operation. Therefore, spatial hole burning causes multi-longitudinal mode operation and competition between higher order modes.

Ring laser cavities can be forced to oscillate in only one of the counter-propagating directions by employing an isolator inside the resonator. The isolator (optical diode) is a combination of a waveplate, a polarizer, and a non-reciprocal material. It lets light to pass in only one direction. With an isolator, there are no standing wave patterns inside the ring resonator. Therefore, spatial hole burning of standing wave cavities are avoided. This leads to lasers that lase in a single longitudinal mode.

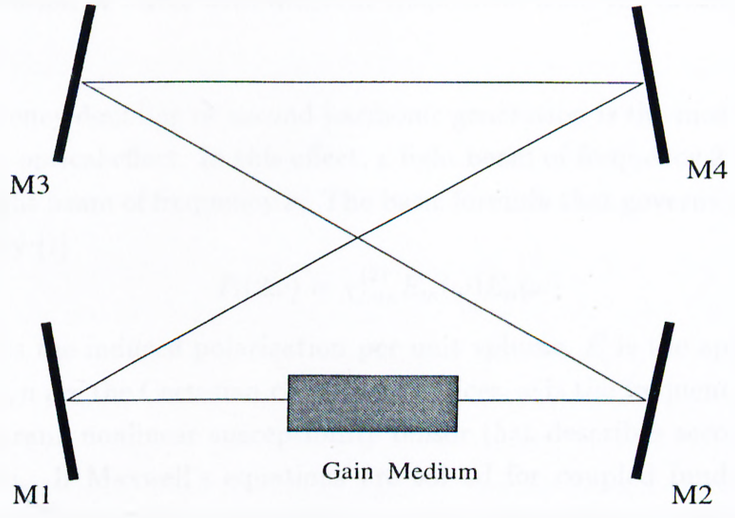

Figure 2.8: A typical four mirror ring laser.

The main disadvantage of ring lasers is that the gain medium is traversed only once. Thus, the laser operates closer to the threshold and have more stringent conditions on internal losses. Also, the beams produced by ring resonators show astigmatic properties because of off-axis reflections from curved cavity mirrors.

The gain and output power calculations of ring lasers are done the same way as for standing wave cavities, except in the former case the gain medium is traversed only once while it is traversed two times in the latter case. The transverse mode calculations for ring resonators are more complex than the

standing wave resonator calculations. These are handled independently in two transverse planes perpendicular to the beam direction (see Appendix B for more detail).

2.4 Frequency doubling

To extend the frequency range of available laser sources, nonlinear optical devices are utilized. When an electromagnetic wave pass through a dielectric medium, a polarization charge density is induced inside the medium. The polarization charge density radiates an electromagnetic wave in response to incoming wave. The relation between the incoming wave and radiated wave is linear for small incoming wave intensities. However, for large intensity incoming waves, the relation becomes nonlinear. This nonlinear relationship causes the generation of waves with different frequencies from the incoming wave frequency.

Frequency doubling or second harmonic generation is the most widely used nonlinear optical effect. In this effect, a light beam of frequency 2ν is produced from a light beam of frequency ν. The basic formula that governs this situation is given by [7]

$$P_l(2\omega) = \chi^{(2)}_{lmn} E_m(\omega) E_n(\omega) \tag{2.40}$$

where P is the induced polarization per unit volume, E is the applied electric field, l, m, n are the Cartesian coordinate indices, ω is the frequency, and $\chi^{(2)}$ is the third-rank nonlinear susceptibility tensor that describes second harmonic generation. If Maxwell's equations are solved for coupled fundamental and second harmonic waves propagating in a nonlinear medium, then the ratio of the power generated at the second harmonic frequency to that of incident at the fundamental frequency is given by [17]

$$\frac{P_{2\omega}}{P_\omega} = \tanh^2 \left[lK^{1/2} \left(\frac{P_w}{A} \right)^{1/2} \frac{sin(\Delta k l/2)}{\Delta k l/2} \right] \tag{2.41}$$

where

$$K = 2\eta^3 \omega_1^2 d_{\text{eff}}^2 \tag{2.42}$$

and

$$\Delta k = \frac{4\pi}{\lambda_1}(n_1 - n_2). \tag{2.43}$$

In these equations, l is the length of the nonlinear crystal, A is the area of the fundamental beam, η is the plane-wave impedance, ω_1 is the frequency of

the fundamental beam, d_{eff} is the effective nonlinear coefficient calculated from propagation direction angles and elements of the tensor $\chi^{(2)}$, n_1 is the index of refraction seen by the fundamental wave, n_2 is the index of refraction seen by the second harmonic wave, and Δk is the phase mismatch between these two waves.

Since for a given wavelength and a given nonlinear material K is a constant, the conversion efficiency depends on the length of the crystal, the power density, and the phase mismatch. For a crystal of fixed length, the second harmonic power is maximum at $\Delta k = 0$ [7]. An effective method of providing equal phases (so $\Delta k = 0$) for the fundamental and second harmonic waves in the nonlinear medium is the utilization of the natural birefringence of uniaxial and biaxial crystals. These crystals have two refractive indices for a given direction of propagation, corresponding to the two allowed orthogonally polarized modes. By an appropriate choice of polarization and direction of propagation it is possible to obtain $\Delta k = 0$. This is called phase matching.

In harmonic generation processes, there are two possible orientations for the linear polarization vectors of beams. If polarization vectors of the beams at frequencies ν and 2ν are perpendicular, it is called type-I process and if the polarization vectors are making an angle of 45°, the process is called type-II.

In our experiments a KTP (Potassium Titanyl Phosphate, $KTiOPO_4$) crystal is used for second harmonic generation. It is widely used with Nd lasers for frequency doubling. It has large nonlinear coefficients, and adequate birefringence in the orthogonal planes that allows type-II phase matching over a large wavelength range. It has wide acceptance angles, an unusually large temperature bandwidth, relatively good thermal properties, and a high damage threshold. Figure 2.9 shows the crystal orientation for type-II phase matched second harmonic generation of Nd:YAG with KTP. In this figure, ϕ is the angle between a-axis of crystal and the direction of propagation.

The efficiency of the second harmonic generation process is strongly dependent on the intensity of the fundamental beam. Frequency doubling can be done by passing the laser beam through the crystal. However, the conversion efficiency will be low in this case, due to the low intensities of the cw laser output beam. The possible solution of this problem is to place the doubling crystal inside the laser resonator where the circulating power is a factor of $1/T$ (T is the transmittivity of the output coupler) larger than the output power. The second harmonic power is then coupled from the cavity by replacing the output coupler with a mirror which has high reflectance at the fundamental

frequency and high transmittance at the second harmonic. This technique is known as intracavity frequency doubling.

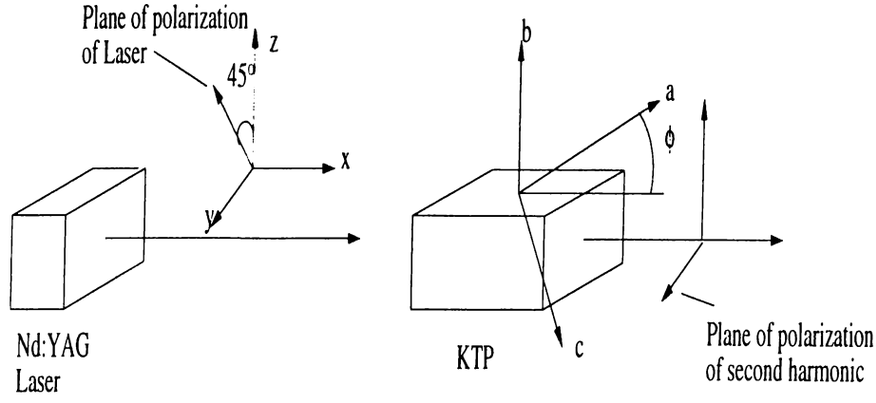

Figure 2.9: Orientation of KTP crystal for type-II interaction at 1064 nm.

2.5 History of experimental work

The first stimulated emission device was implemented in 1954 by Charles H. Townes, J. P. Gordon and H. Zeiger at Columbia University. It was an ammonia beam maser oscillating at 24 GHz. The extension of microwave maser concepts to the optical frequencies (laser) came immediately. The first paper discussing the possibility of realization of the optical masers was published by Schawlow in 1958 [18]. This paper set some of the fundamental considerations for laser action. The first successful laser operation emerged in 1960 [1]. This was a flash-lamp-pumped ruby laser operating at 694 nm built by Theodore H. Maiman at Hughes Research Laboratories. An enormous number of laser devices have emerged since the first successful laser.

Newman [19] was the first one who mentions the use of semiconductor sources to pump a solid-state laser. He stated that radiation near 808 nm from recombination in GaAs diodes, essentially an LED, could excite fluorescence near 1.06 μm in Nd:$CaWO_4$. After this, Keyes and Quist [20] implemented the first diode laser-pumped solid-state laser after the development of the first GaAs diode lasers [21]. This was a $CaF_2:U^{3+}$ laser operating at 2.613 μm.

After these early efforts, interest shifted to Nd:YAG lasers because the Nd^{3+} ion has excellent spectroscopic properties for diode pumping. There is strong absorption of Nd:YAG at the emission bands of GaAs, GaAlAs and GaAsP diode lasers. The first diode laser-pumped Nd:YAG laser was demonstrated by

Ross [22]. It was side-pumped by a single GaAs diode laser. This was followed by a number of reports of side pumped Nd:YAG lasers [23]-[27].

There were also studies on end-pumped lasers in addition to side-pumped ones. The first end-pumped Nd:YAG laser was reported by Rosenkrantz in 1973 [28]. This was a pulsed laser end-pumped by a GaAs diode laser. Simple expressions were derived for the threshold pump energy in pulsed mode in this report. Other efforts on end-pumped lasers followed this one [29]-[32]. With improvements in diode laser technology in the early 1980's allowing higher powers. progress was made in end-pumped Nd:YAG systems. Sipes [33] showed the highest reported wall-plug efficiency of 8% for a cw Nd:YAG laser up to that date. 80 mW cw power was achieved with only 1 W of electrical power input to a single diode laser pump. Since then, the efficiency and output power of end-pumped Nd:YAG lasers have increased steadily. By better coupling the diode laser's beam into the Nd:YAG crystal, Berger [34] reported 10.8% at 415 mW cw. In 1991, Shannon [35] demonstrated a Nd:YAG laser end-pumped by a 10 W laser diode bar with 1.9 W output power. Then 92 W multimode and 60 W TEM_{00} mode output powers were reported by Tidwell [36].

As the power levels increased, the interest for second harmonic generation progressed. Baer [37] showed a laser originally proposed by Sipes [33] could be intracavity doubled with good efficiency by using a KTP crystal. Many reports have been published showing intracavity second harmonic generation with diode end-pumped Nd:YAG lasers [38]-[40].

First single-frequency operation of a cw lamp-pumped Nd:YAG ring laser was reported by Clobes [41] in 1972. Earliest versions of the diode-pumped Nd-YAG ring lasers were monolithic designs (consists only of a specially shaped crystal) [42], [43]. Later, discrete element diode-pumped ring lasers were reported [44]-[46]. Some were also intracavity frequency doubled [45], [46].

Chapter 3

PUMPING OF THE LASER

The block diagram of our laser is shown in Figure 3.1. Light from a diode laser is used to optically pump the gain medium which is an Nd:YAG rod. Various optics are used to shape the pump light to provide appropriate coupling of the pump beam to the gain medium. An optical resonator provides the necessary feedback for laser action. The front mirror of the resonator serves as an output coupler for the Nd:YAG laser. This chapter describes the pumping scheme that we have employed in our experiments.

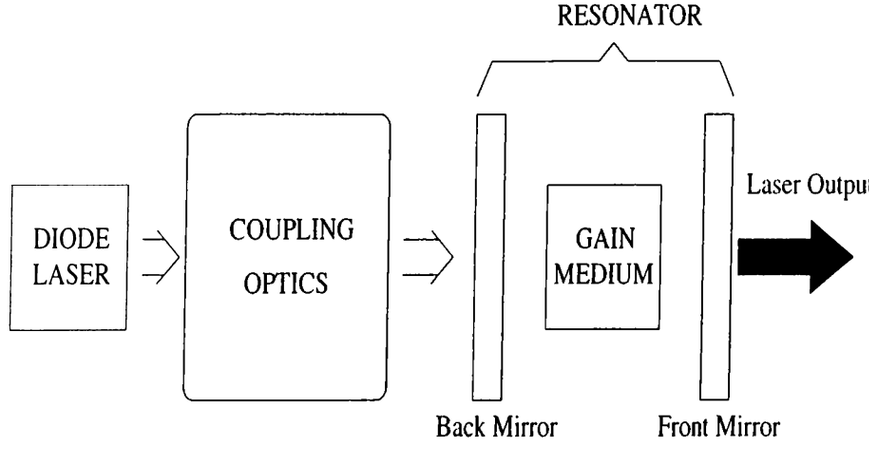

Figure 3.1: Simple block diagram of the laser.

3.1 Diode laser

The laser used as a pump source in our experiments is SDL-2382-P1 manufactured by Spectra Diode Laboratories. It is rated to supply up to 4 W continuous wave (cw) power (see Figure 3.2). These lasers are produced by a metalorganic chemical vapor deposition (MOCVD) technique. MOCVD growth allows fabrication of quantum wells in the diode active layer, increasing electrical-to-optical-efficiency and lowering threshold current requirements. This model also has broad area lateral index guided structure which uses lateral refractive index variations for confinement of photons in the active region, thus increasing efficiency.

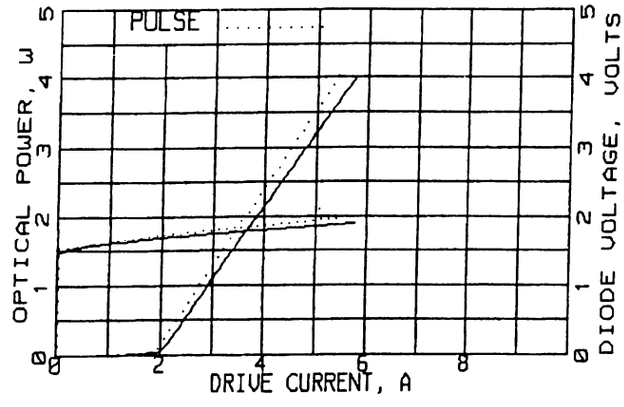

Figure 3.2: Input output relation of the laser diode. The curve starting from the 2 A point corresponds to optical power. The other curve corresponds to diode voltage.

Our diode laser has a wavelength range of approximately 797 to 815 nm that can be tuned by adjusting its temperature. The temperature coefficient that relates the change in emission wavelength to the diode temperature is approximately 0.3 nm/°C. Our diode laser is packaged with a thermoelectric (TE) cooler, which allows us to adjust the diode temperature and achieve optimum absorption in the gain medium. The spectral width of the laser is rated to be less than 2 nm full-width at half-maximum (FWHM).

The input current of the diode and the temperature of the TE cooler are controlled by a combination current source/temperature controller, LDC-3752 Laser Diode Controller manufactured by ILX Lightwave Corporation. The current source provides a high stability output with multiple laser protection features. The built-in temperature controller can work with TE modules to deliver precision laser temperature control over a wide range of temperatures.

The emitting area of the laser diode has a length of 500 μm and width of 1 μm. Because of this unequal aspect ratio, the emitted light has different divergence angles in the horizontal and vertical planes (see Figure 3.3). The divergence angle in the plane parallel to the junction is 12°, whereas it is 34° in the plane perpendicular to the junction.

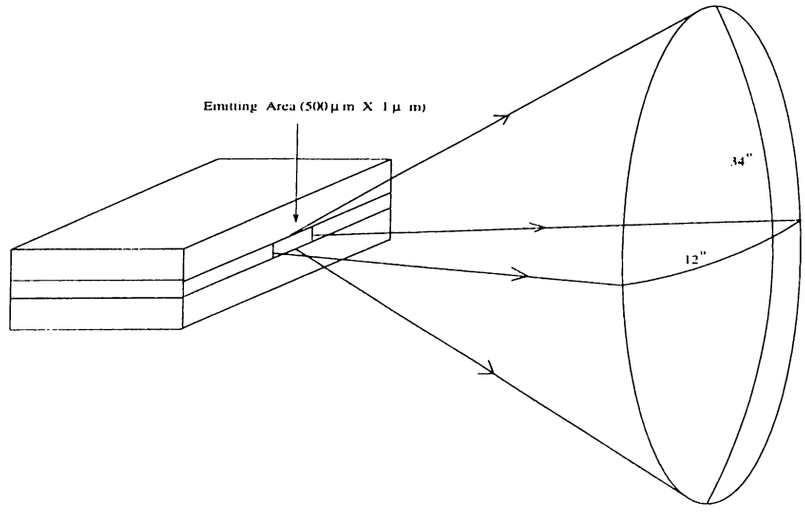

Figure 3.3: Divergence angles of the output beam of the laser diode.

Apart from different divergence angles in the two perpendicular planes, the beam of the laser diode also exhibits astigmatism, i.e. the locations of beam waists at the horizontal and vertical planes are different. The beam waist is located at the surface of the output facet in the plane perpendicular to the junction which is index guided. However, the broad area plane that is parallel to the junction has a beam waist located 1 mm behind the front facet.

The diode laser radiates with a near Gaussian distribution in the plane perpendicular to the junction, and a more complex pattern in the plane parallel to the junction. Figure 3.4 shows the typical far field radiation pattern in two perpendicular planes. The near field, on the other hand, consists of two active segments separated by an isolation space, resulting in two independent lobes of radiation.

The polarization ratio of the diode laser beam, the ratio of the light polarized parallel to the junction to the light polarized perpendicular to the junction, is better than 20:1.

The diode is mounted on a heat sink that dissipates excess heat. This mounting arrangement results in an orientation such that the plane parallel to

the diode junction is perpendicular to optical table.

For more information on the diode laser see Appendix C.

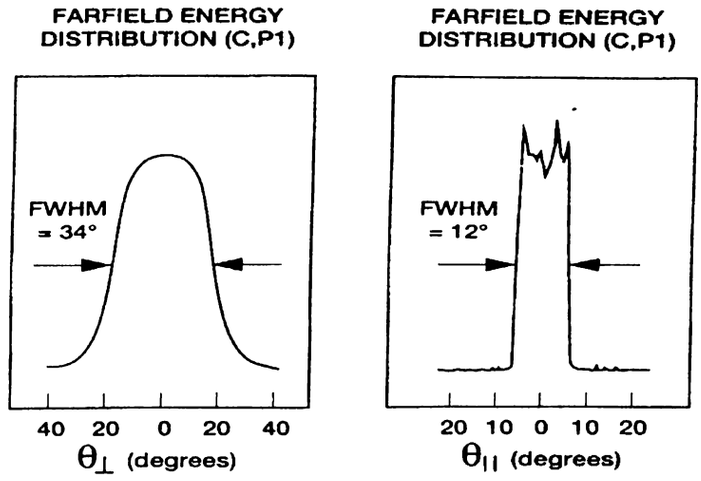

Figure 3.4: Typical far field radiation pattern of laser diode beam in two perpendicular planes.

3.2 Coupling optics

There are two requirements that must be met for an efficient diode-end-pumped laser. First, the gain medium must be long enough to absorb a large fraction of the pump light. Second, the pump spot size must be less than or equal to the mode size [8]-[10]. These requirements set restrictions on the pump beam divergence angle and the pump spot size. In order to satisfy these restrictions on the pump beam, the coupling optics section should be designed carefully.

The coupling optics are shown in Figure 3.5. Right after the diode laser, we put a high numerical aperture (NA = 0.615) lens to collect as much light from the diode as possible. This is a composite lens with focal length of 6.5 mm (Melles Griot 06 GLC 001). We measure 3.9 W power at the output of this lens at full diode current. This corresponds to an estimated loss of 2.5% at the collimating lens. Because of astigmatism, the resulting beam is well collimated in the horizontal plane, but has a divergence of 2.2° (half angle) in the vertical plane. A cylindrical lens with a focal length of 30 cm is used to collimate the beam in this plane. The cylindrical lens inserts 10.5% loss due to reflections at the lens surfaces.

After the cylindrical lens, we have a beam that is collimated in both planes. It has a width of 24 mm in the vertical and 8 mm in the horizontal. This beam is focused into the Nd:YAG rod with a spherical lens of 5 cm focal length. The intensity distribution at the focal plane is imaged by a CCD camera. A contour plot of this intensity distribution is given in Figure 3.6. The contour which corresponds to an intensity that is $1/e^2$ of the peak intensity is shown in Figure 3.7. The spherical lens introduces an additional loss of 8% due to surface reflections.

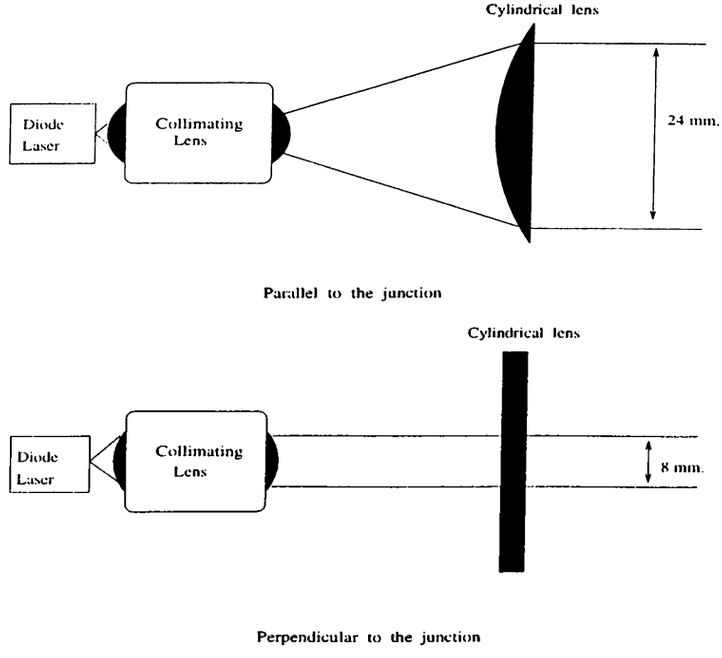

Figure 3.5: Coupling optics.

As seen from Figure 3.7, the beam spot is approximately 600 μm long in one plane while 100 μm in the other. This difference is caused by the different radiation characteristics of the diode laser output beam in these two planes.

When the pump beam or the intracavity laser beam pass through the gain medium, surface reflections induce losses. To eliminate these losses, one can either use anti-reflection coatings or laser rods that have faces cut at Brewster's angle. Using the Brewster's angle cut rods has the additional advantage of inducing differential loss between s and p-polarized laser modes, thus achieving a linearly polarized laser output.

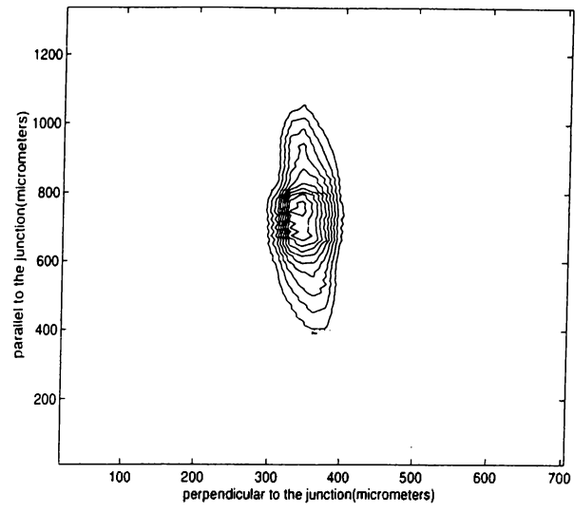

Figure 3.6: Contour plot of the intensity distribution of the pump beam at the focal plane obtained by a CCD camera.

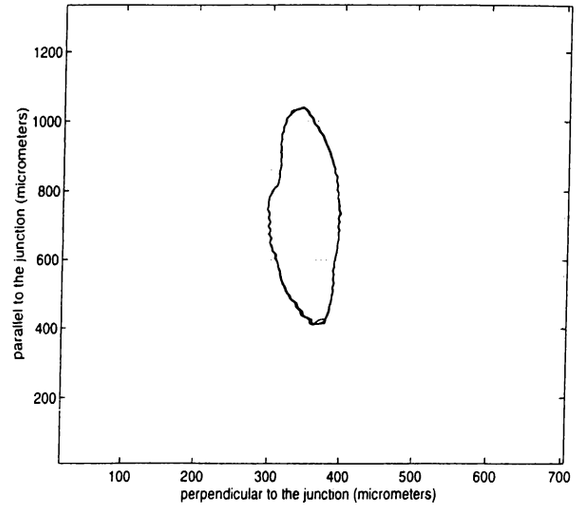

Figure 3.7: The $1/e^2$ contour plot of the intensity distribution of the pump beam at the focal plane obtained by a CCD camera.

To couple the pump beam to the Brewster's angle cut rod in our design, we have to rotate the polarization of the diode light by 90°. An easy way of doing this is to rotate the diode by 90°. However, the plane in which the pump beam spot is 600 μm long (see Figure 3.7) becomes parallel to the Brewster's angle cut plane in this case. Upon entering the rod, the length in this plane is multiplied by a factor of 1.82 because of oblique angle of incidence, resulting in a 1090 μm long spot. This figure exceeds the desired laser mode sizes in the gain medium. Therefore we have adopted another method. We position a

$\lambda/2$ waveplate after the collimating lens to rotate the polarization. After the waveplate we measured the extinction ratio to be 20:1. The addition of the waveplate inserts 10.3% loss to the pump beam, since it is not anti-reflection coated at the appropriate wavelength.

3.3 Gain medium

The laser gain medium is an Nd:YAG (neodymium-doped yttrium aluminum garnet) crystal in our experiments. The Nd:YAG crystal is a cylindrical rod that is 10 mm long and 3 mm in diameter. With this length, 98% of the incoming pump light is absorbed along the crystal. The end surfaces are cut at Brewster's angle to minimize reflections. We placed the crystal in an aluminum heat sink to decrease thermal loading. We wrapped the surface of the Nd:YAG rod with a layer of indium foil to increase heat conduction from the crystal to the heat sink.

Nd:YAG is one of the most commonly used solid state laser materials in science and technology. It has very favorable optical and physical properties. YAG ($Y_3Al_5O_{12}$) is the host material. It is a hard, colorless, optically isotropic crystal and has a high thermal conductivity. A few percent of Y^{3+} is substituted by Nd^{3+} to obtain Nd:YAG. The amount of Nd^{3+} in the crystal used in our experiments is 1%. Some of the properties of Nd:YAG are listed in the following table [7].

Chemical formula	Nd: $Y_3Al_5O_{12}$
Atomic % Nd	1.0
Nd atoms/cm^3	1.38 x 10^{20}
Melting point	1970°C
Density	4.56 g/cm^3
Linewidth	0.45 nm
Stimulated emission cross section R_2 - Y_3 $^4F_{3/2}$ - $^4I_{11/2}$	 σ_{21} = 6.5 x 10^{-19} cm^2 σ_{21} = 2.8 x 10^{-19} cm^2
Spontaneous fluorescence lifetime	230 μs
Photon energy at 1064 nm	$h\nu$ = 1.86 x 10^{-19} J
Index of refraction	1.82 (at 1.0 μm)
Absorption coefficient @808.5 nm	3.8 cm^{-1}

Table 3.1: Physical and optical properties of Nd:YAG.

The Nd:YAG laser at 1064 nm is a four-level system. Its energy level diagram is depicted in Figure 3.8 [7]. At room temperature, the strongest transition is at 1064 nm so that highest gain occurs at that wavelength. There are also other possible lasing wavelengths. The most notable ones are 1300 and 946 nm transitions. Main pump bands are around 810 and 750 nm. The lower laser level is 9.42×10^{-31} J above the ground state. Therefore, the population density of this level is $\exp(\Delta E/kT) \simeq \exp(-10)$ times the ground-state density at room temperature. Figure 3.9 [7] shows the fluorescence spectrum of Nd:YAG near 1064 nm. The absorption spectrum of Nd:YAG is given in Figure 3.10 [7].

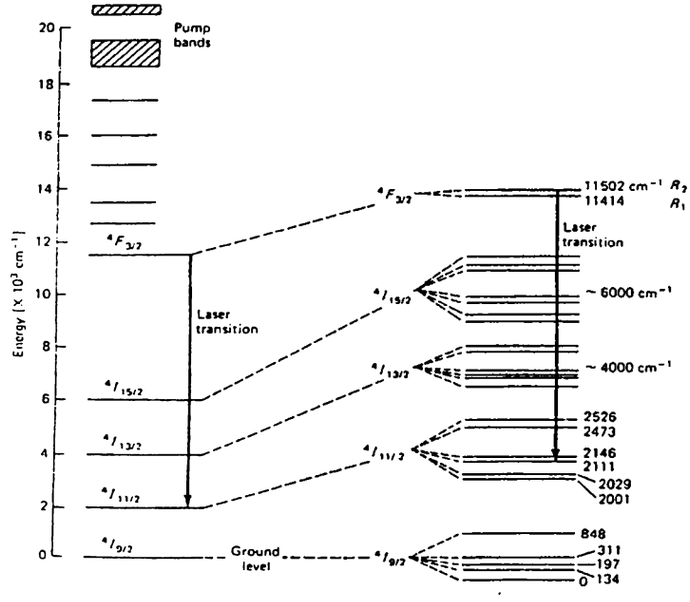

Figure 3.8: Energy level diagram of Nd:YAG.

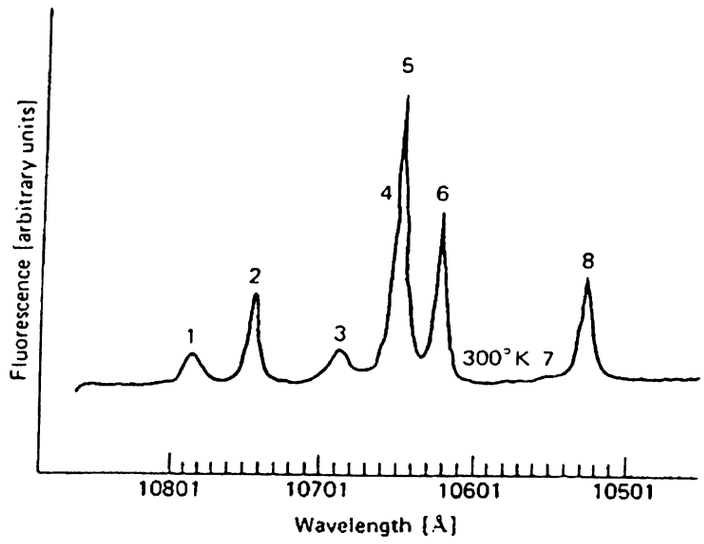

Figure 3.9: Fluorescence spectrum of Nd:YAG at 300 K near 1064 nm.

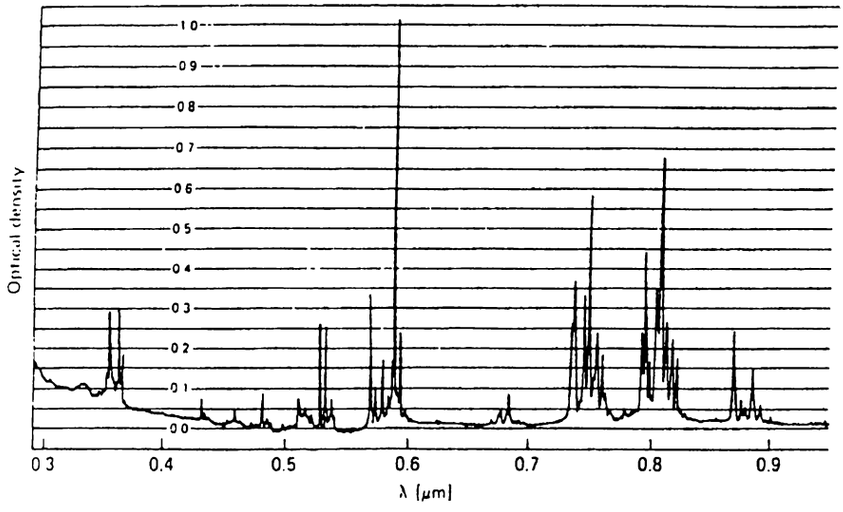

Figure 3.10: Absorption spectrum of Nd:YAG at 300 K.

Chapter 4

FABRY-PEROT RESONATOR DESIGNS

A Fabry-Perot resonator is an optical structure composed of two mirrors facing each other. We implemented different lasers with various Fabry-Perot resonators (see Figure 4.1). We constructed these different resonators by changing the front and back mirrors or changing the distance between them (resonator length). The mirrors we used in these experiments are listed in Table 4.1. All these mirrors add approximately 10% loss to the pump beam when used as an input coupler to the laser because of surface reflections.

R(cm)	Reflectance & Coatings
flat	HR @1064nm, HT @808nm
flat	93% @1064nm
flat	90% @1064nm
flat	87% @1064nm
-20	HR @1064nm
-25	HR @1064nm
-50	HR @1064nm
-10	HR @1064nm, HT @808nm
-300	HT @532nm

Table 4.1: The list of mirrors used in the experiments. HT means the mirror is coated for high transmission and HR means it is coated for high reflection at the specified wavelength. R is the radius of curvature for the mirrors.

The curved mirrors (-50, -25, -20 and -10 cm) are used as input couplers. Changing the mirror radii affects the mode radius in the resonator. Therefore,

we can investigate the laser performance for different mode radii. As output couplers we used flat mirrors with different reflectivities (93%, 90%, 87%).

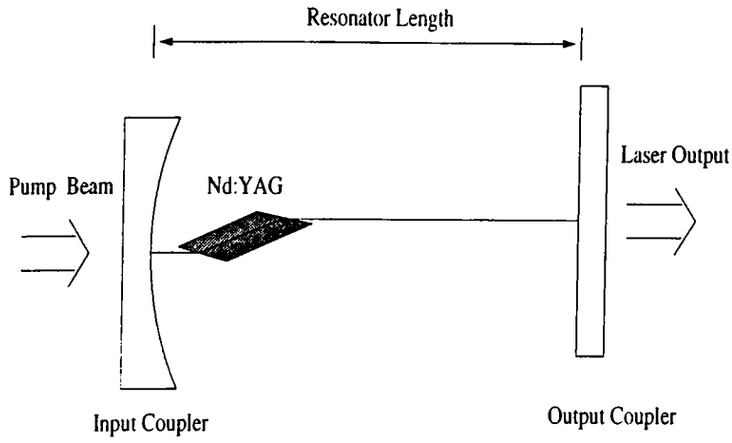

Figure 4.1: The Fabry-Perot laser.

At first, we kept the resonator length fixed at 7.3 cm and implemented all the input and output coupler combinations. The resonator lengths mentioned are the actual distances between the input and output couplers. The optical path length (which the beam traverses) is slightly longer than this distance because of the geometry (the Brewster's angle cut Nd:YAG) and the refractive index of the Nd:YAG crystal.

4.1 Input couplers

The input output relations for the lasers with different input couplers are given in Figures 4.2 through 4.5. Results show linear relationships between input and output powers for all the lasers except for the laser with the -20 cm input coupler. We observed a nonlinear input-output characteristic with this laser. At two points (Pin = 2.2 W and Pin = 1.8 W), there are increases in output power while the input power is reduced. At these points, we also observed instant changes in the laser output mode profile. Therefore, a possible explanation of this nonlinearity could be higher order transverse mode competition at these power levels.

For ease of comparison, the characteristic properties of these lasers are summarized in Tables 4.2 through 4.4.

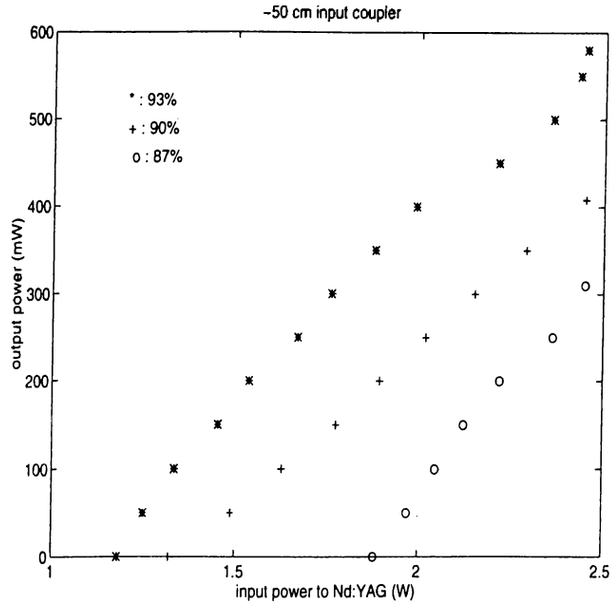

Figure 4.2: Laser output power versus optical power incident to Nd:YAG for the laser with -50 cm input coupler.

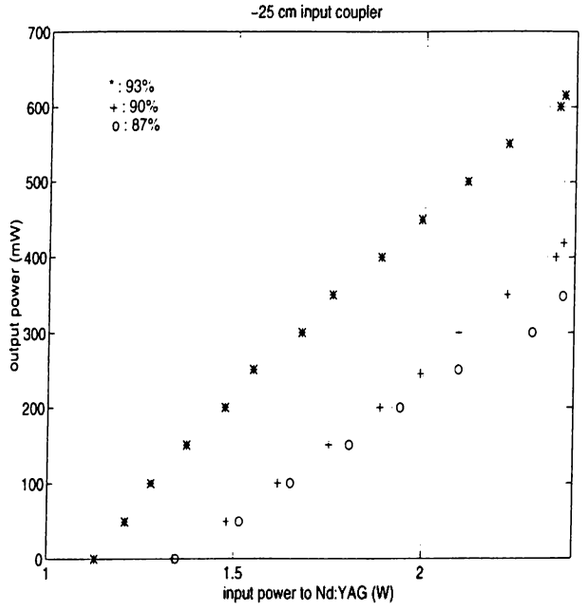

Figure 4.3: Laser output power versus optical power incident to Nd:YAG for the laser with -25 cm input coupler.

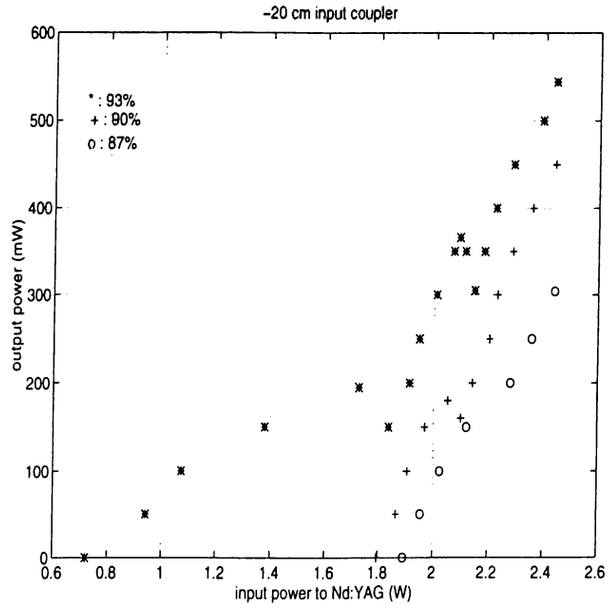

Figure 4.4: Laser output power versus optical power incident to Nd:YAG for the laser with -20 cm input coupler.

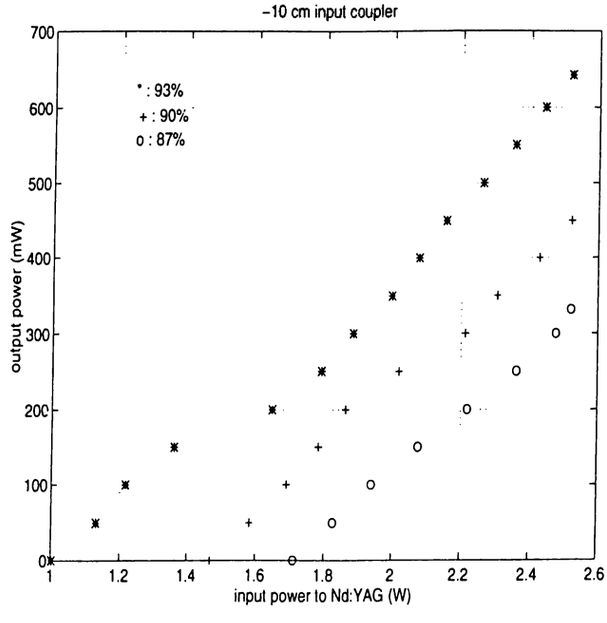

Figure 4.5: Laser output power versus optical power incident to Nd:YAG for the laser with -10 cm input coupler.

Input coupler	-50 cm	-25 cm	-20 cm	-10 cm
Max. output power (mW)	580	615	540	640
Slope efficiency	0.45	0.50	0.32	0.46
Threshold (W)	1.2	1.1	0.7	1.1
Optical conversion eff. (%)	24	26	22	25
Wall-plug efficiency (%)	5.3	5.6	4.9	5.9

Table 4.2: Properties of lasers with 93% output coupler.

Input coupler	-50 cm	-25 cm	-20 cm	-10 cm
Max. output power (mW)	410	420	450	450
Slope efficiency	0.36	0.40	0.68	0.44
Threshold (W)	1.3	1.3	1.8	1.5
Optical conversion eff. (%)	17	18	18	18
Wall-plug efficiency (%)	3.8	3.9	4.1	4.1

Table 4.3: Properties of lasers with 90% output coupler.

Input coupler	-50 cm	-25 cm	-20 cm	-10 cm
Max. output power (mW)	310	350	305	330
Slope efficiency	0.54	0.34	0.54	0.44
Threshold (W)	1.9	1.3	1.9	1.7
Optical conversion eff. (%)	13	15	12	13
Wall-plug efficiency (%)	2.8	3.2	2.8	3.0

Table 4.4: Properties of lasers with 87% output coupler.

Maximum powers are measured at the diode current of 5752 mA. The output power of the diode is 4 W and the diode voltage is 1.89 V at that current level. Therefore the input electrical power to diode at 4 W output is 10.9 W.

A maximum output power of 640 mW is obtained from the laser with the -10 cm input coupler and the 93% output coupler. This laser also has the maximum wall-plug efficiency of 5.9%. However, the maximum optical conversion efficiency of 26% is obtained from the combination of the -25 cm input coupler and the 93% output coupler. The laser with the -20 cm input coupler and the 93% output coupler has the minimum threshold of 0.7 W. The slope efficiency is maximum for the laser with the -20 cm input coupler and the 90% output coupler with the value of 68%.

As seen from the figures and tables, the output powers of all the lasers increase when the reflectance of the output coupler increases. For the laser

with the -10 cm input coupler, the output power and transmittance relation is given in Figure 4.6. Also, a typical output power versus transmittance of the output coupler graph is given in Figure 4.7. From these two figures, we can infer that the optimum output coupler for this laser is greater than or equal to 93%.

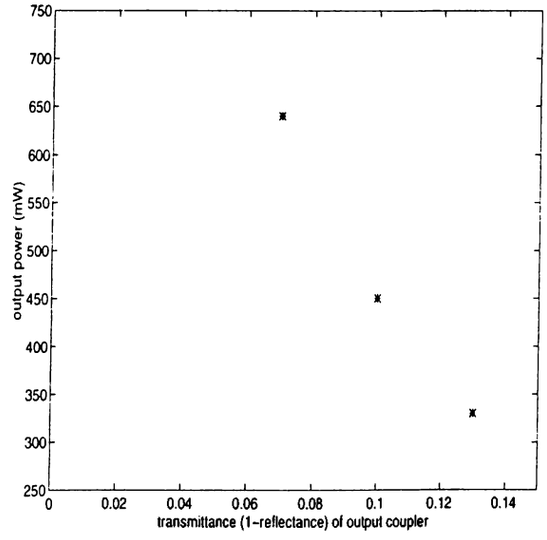

Figure 4.6: Output power versus the transmittance of the output coupler for the laser with -10 cm input coupler.

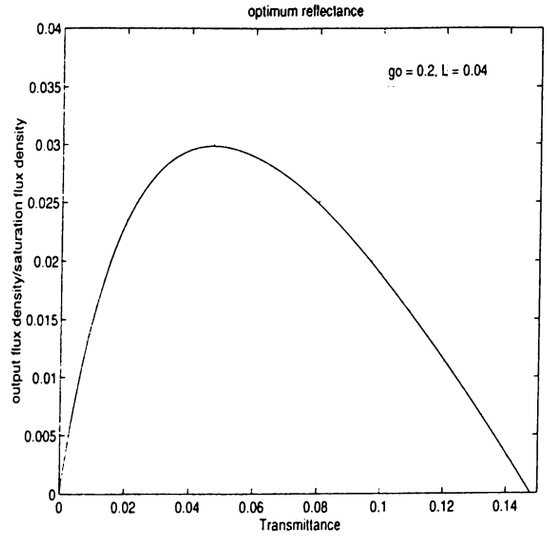

Figure 4.7: Output power versus the transmittance of the output coupler for a typical laser with $g_o = 0.2$ and $L = 0.04$.

To find the optimum output coupler transmittance exactly, γ_o (unsaturated

gain coefficient) and L (useless losses) must be known. These can be determined by using output couplers with different reflectivities and plotting the threshold power for each coupler [6]. Extrapolation of the straight line plot of $-\ln R$ versus P_{TH}, at $P_{TH} = 0$, yields the the round-trip resonator loss L. The slope of the straight line is $2K$ which is a factor giving $g_0 = 2\gamma_0 d = 2KP_{in}$. Figure 4.8 shows these relations for the laser with the -10 cm input coupler. From this figure, the resonator losses are found to be $L = 0.05$. The slope equals 0.107 and it gives $g_0 = 0.017$ x 2.52 = 0.27. From this data, the optimum output coupler reflectance is found to be 93.4% which is very close to our output coupler reflectance. Figure 4.9 shows the same relationships for the laser with the -50 cm input coupler. The useless loss for this laser is 0.02, g_0 is determined as 0.22 and they give the optimum output coupler reflectance as 95.4%. The data for the lasers with the -25 cm and the -20 cm input couplers are given in Figures 4.10 and 4.11. Proper extrapolations which give the optimum output coupler reflectance can not be drawn in these figures. For the laser with the -20 cm input coupler, the nonlinear input-output characteristic (see Figure 4.4) gives difficulty in determining the threshold powers. For the -25 cm input coupler, the threshold powers of the lasers with the 90% and the 87% output couplers are the same. This is also a kind of nonlinearity possibly caused from higher order mode competitions or thermal effects.

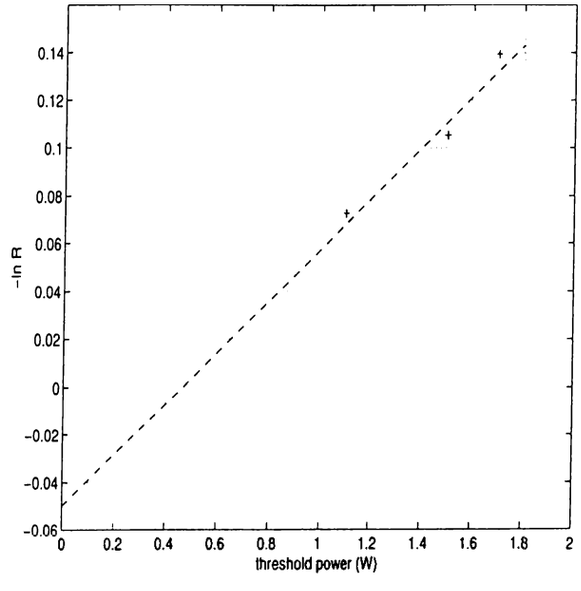

Figure 4.8: -ln(R) versus threshold power for the laser with -10 cm input coupler.

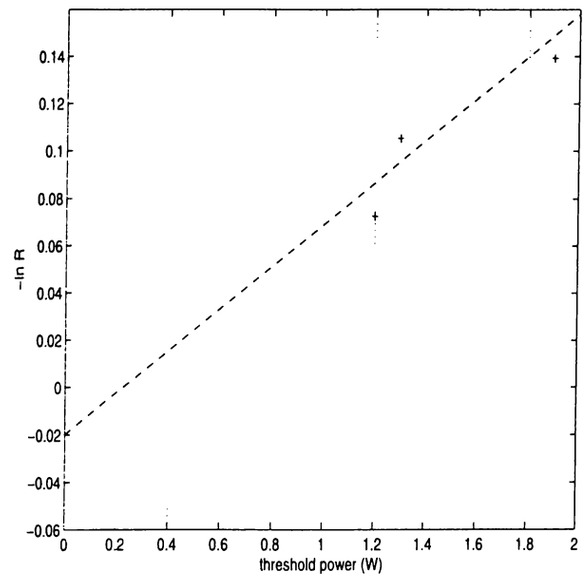

Figure 4.9: -ln(R) versus threshold power for the laser with -50 cm input coupler.

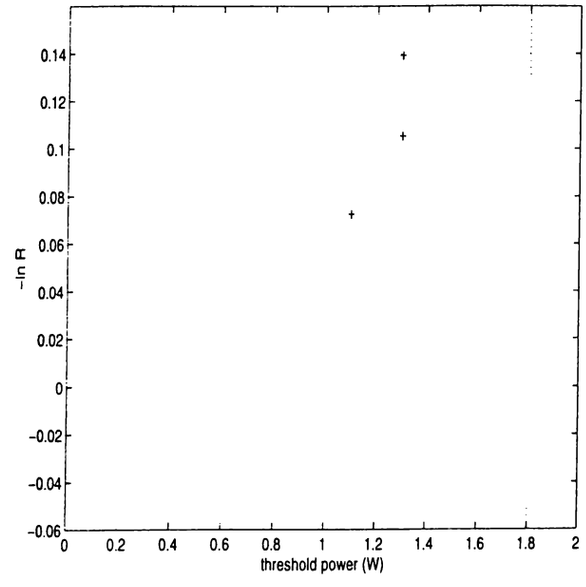

Figure 4.10: -ln(R) versus threshold power for the laser with -25 cm input coupler.

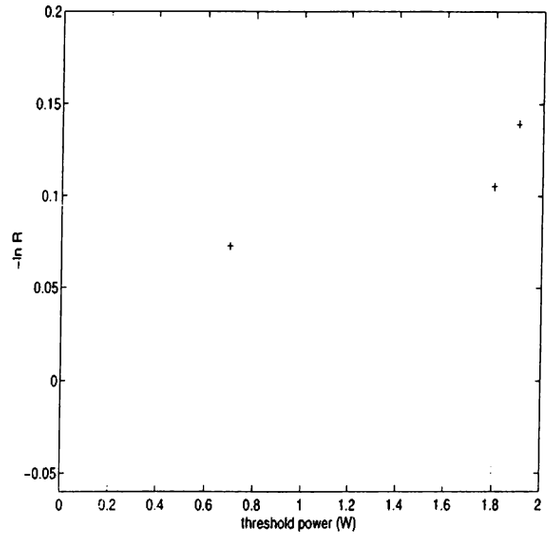

Figure 4.11: -ln(R) versus threshold power for the laser with -20 cm input coupler.

Except for the -20 cm input coupler laser, the maximum output power increases as the radius of curvature of the input coupler decreases. The decrease of the radius of curvature results in a decrease of the mode radius inside the Nd:YAG. Therefore, the decrease in the mode radius causes an increase of the output power (see Figure 4.12). We can infer that the pump beam and the laser mode are best coupled when the mode radius is around 230 μm for this laser configuration.

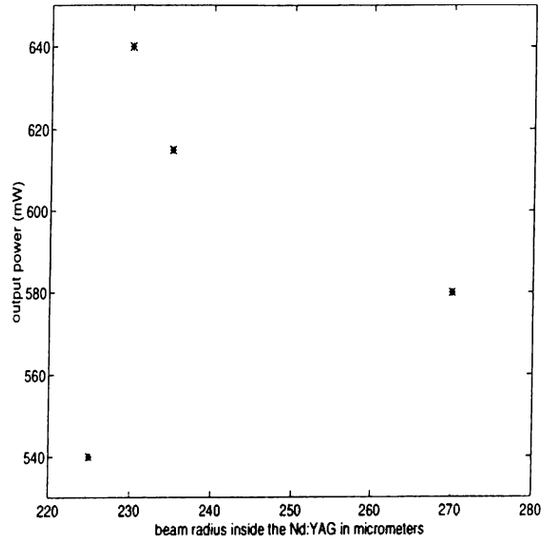

Figure 4.12: Output power versus beam radius relation for the laser with 93% output coupler.

To fortify this interpretation, we carried out further measurements. In these, with different input couplers we varied the resonator length and measured the maximum powers. The stability region, in terms of the resonator length, of the laser with the -10 cm input coupler is very different from the other lasers. Therefore, we took two sets of measurements. The measurements with the -20, -25, and -50 cm input couplers are given in Table 4.5. Figure 4.13 shows the relationship between the resonator length and output power of the laser with the -10 cm input coupler. The data in the table support our previous conclusion that as the mode radius is reduced the coupling between the mode and pump beam increases, so the output power increases. From the -10 cm input coupler data, we can see that beyond the optimum mode radius which is 210 μm (corresponds to 6 cm resonator length), the output power decreases. When we put two mirrors so close to each other, the output power again increases. However, in this case the output beam has very bad characteristics, it is multimode and has a large divergence angle.

	-50cm		-25cm		-20cm	
Res. length (cm)	Beam rad. at YAG(μm)	Pout (mW)	Beam rad. at YAG(μm)	Pout (mW)	Beam rad. at YAG(μm)	Pout (mW)
7.3	270	580	235	610	230	550
9.8	288	510	251	430	250	490
12.1	307	397	275	380	280	350
14.9	330	130	310	210	335	-

Table 4.5: Resonator length versus P_{out}.

Since the maximum power is obtained with the -10 cm input coupler at a resonator length of 6 cm, we present the input output graph of this laser in Figure 4.14. The maximum power obtained for this configuration is 780 mW with the 93% output coupler. Optical conversion efficiency is 31%, threshold power is 0.54 W, slope efficiency is 0.41 and wall-plug efficiency is 7.2%. The maximum power with 90% output coupler is 640 mW, optical conversion efficiency is 25%, threshold power is 0.79 W, slope efficiency is 0.36 and wall-plug efficiency is 5.9%. For 87% output coupler we obtained 510 mW output power. Its optical conversion efficiency is 20%, threshold power is 0.89 W, slope efficiency is 0.33 and wall-plug efficiency is 4.7%.

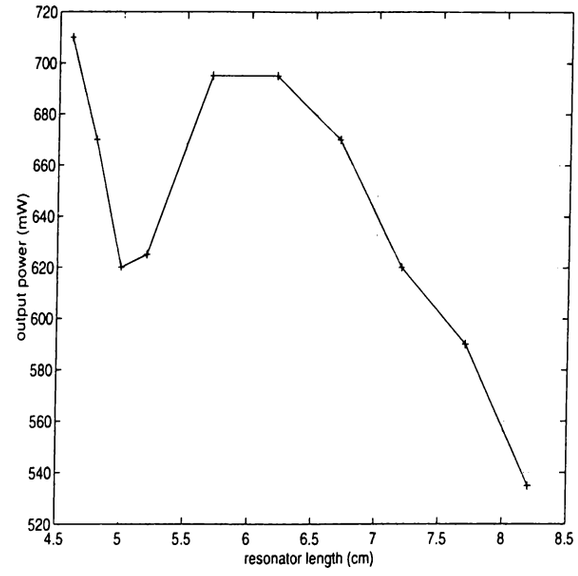

Figure 4.13: Resonator length versus output power for the laser with -10 cm input coupler.

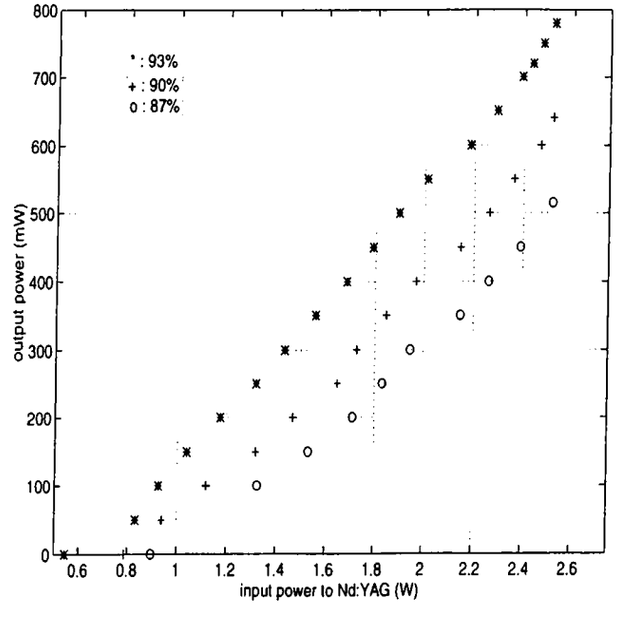

Figure 4.14: Laser output power versus optical power incident to Nd:YAG for the laser with -10 cm input coupler. Resonator length is 6 cm.

Constructing a laser with two planar mirrors at a very short resonator length is a common technique to couple out very large fractions of the stored energy inside the Nd:YAG. However, this cannot be used as an ordinary laser because of the poor optical properties of the output beam (multimode, large divergence angle). To see the maximum power obtained from our laser, we also implemented this kind of resonator. The input coupler is a flat mirror that

is high transmitting at 808 nm and high reflecting at 1064 nm. The output couplers are flat mirrors with different reflectances (93%, 90%, 87%). The resonator length is only 2 cm. The input output characteristic of this resonator is shown in Figure 4.15. Maximum power of 1.06 W is obtained with 93% output coupler. The optical efficiency that corresponds to this figure is 42%. This is a rather high figure because theoretically maximum optical efficiency which can be obtained in such a laser is 76%, where there are no losses and all the pump photons are converted to laser photons.

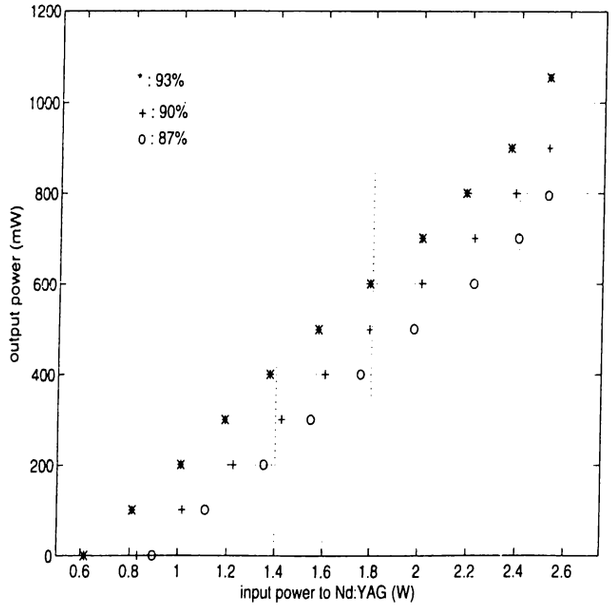

Figure 4.15: Laser output power versus optical power incident to Nd:YAG for the resonator with two flat mirrors and 2 cm resonator length.

4.2 Pump wavelength and laser performance

As mentioned before, the output wavelength of the diode laser can be adjusted by changing its temperature. Therefore, it is possible to maximize the absorption of crystal by overlapping the output wavelength of the diode with the absorption spectra of Nd:YAG. To achieve this, we focused the pump light to the crystal and measured the normalized transmitted power versus diode temperature. This data is given in Figure 4.16. It is clearly seen that at 20°C the absorption is maximum. When we constructed the laser, we did a similar experiment. In this case, we measured the normalized output power of the laser versus the temperature of the diode laser. Figure 4.17 shows this data.

This time the output power is maximized at 7°C, and it does not vary much between 15°C and 20°C. To explain this seeming discrepancy we needed the output wavelength of the diode at specific temperatures. We measured the diode output wavelength by changing its temperature. This is shown in Figure 4.18. As seen from the graph, the center wavelength of the diode output at 20°C is at 808.5 nm at where Nd:YAG has its absorption peak. Therefore, the absorption coefficient of the crystal is maximum at 20°. At 7°C the center wavelength is around 804 nm, so the absorption coefficient of the crystal is less than the value at 20°C. Hence, the diode light is absorbed in a longer distance. This spreads the gain in a longer distance and the gain medium becomes less saturated. As a result, the total gain at 7°C becomes larger than the value at 20°C. Therefore, the output power of the less saturated gain medium is greater than that of the more saturated gain medium.

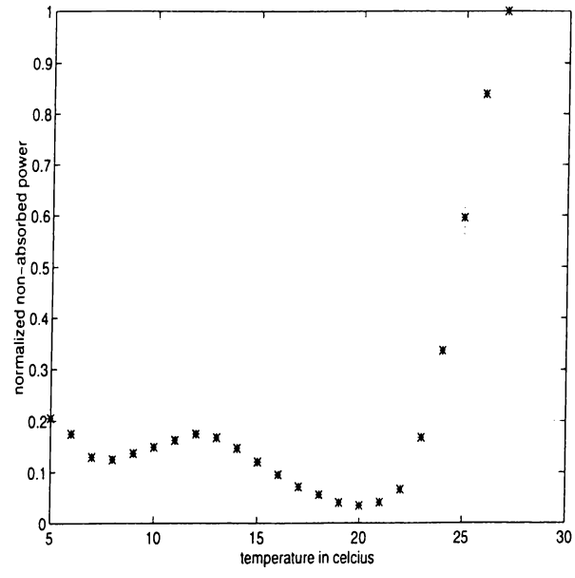

Figure 4.16: Normalized transmitted power through Nd:YAG versus diode laser's temperature.

We did all the experiments (if not otherwise stated) at a diode temperature of 15°C because there is a local maximum at 15°C (see Figure 4.17). Also, when operating the diode at full power below 10°C the current limit of the TE cooler is exceeded.

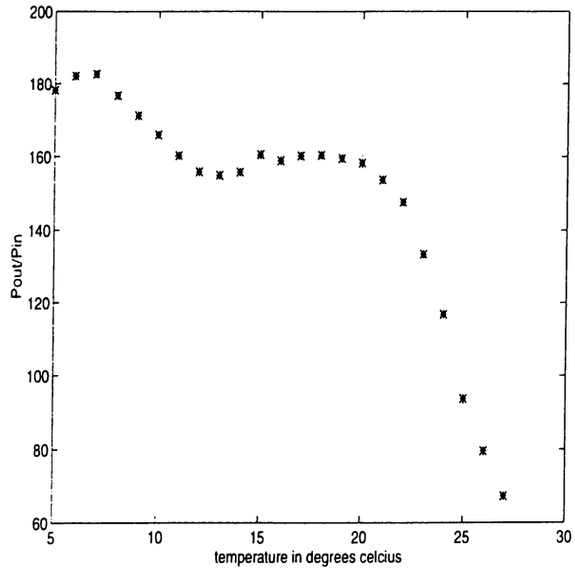

Figure 4.17: Laser output power versus diode temperature.

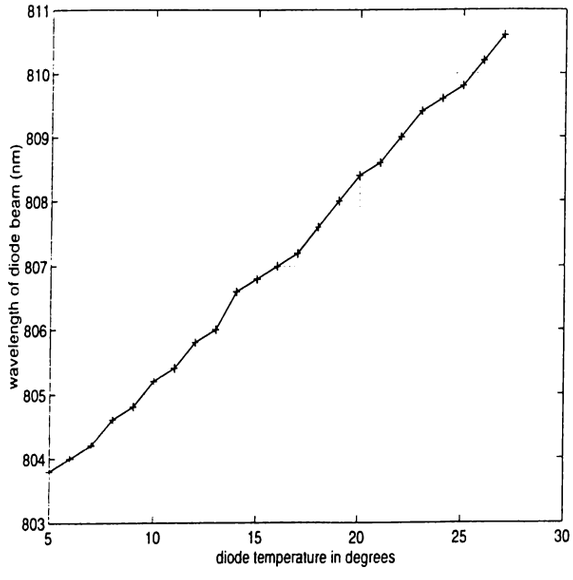

Figure 4.18: Wavelength of diode beam versus diode temperature.

4.3 Efficiency

The losses that the pump beam experiences are shown schematically in Figure 1.19.

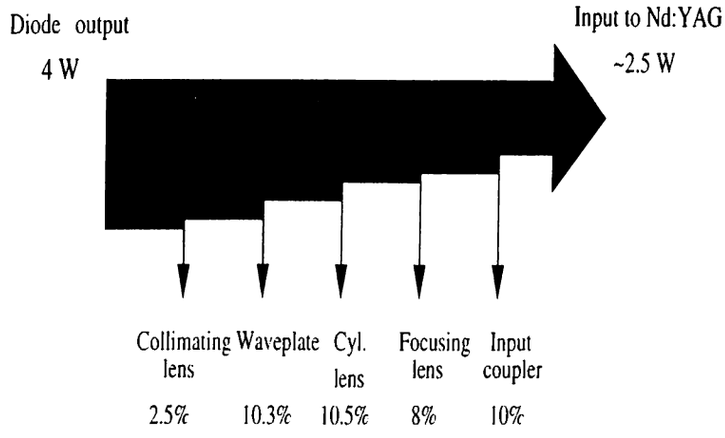

Figure 4.19: Losses of the system.

Although our diode laser has 4 W output power, we could transfer only 2.5 W of it to the Nd:YAG crystal. The overall loss due to surface reflections is 37.5%, which is very high for a typical diode end-pumped laser. The reason for these high losses is that the optics used to transfer the light of the diode to the crystal do not have special anti-reflection coatings.

The pump power of 2.5 W incoming to the Nd:YAG crystal is absorbed in a length of 1 cm. The absorption coefficient of the crystal at 808.5 nm (diode temperature of 20°C) is 3.8 cm^{-1}. The absorption coefficient at 806.5 nm (diode temperature of 15°C) is calculated from the ratio of the absorbed powers at 806.5 nm and at 808.5 nm with the help of Figure 4.16. It is found to be 2.6 cm^{-1}. The pump photon-flux density along the crystal can be written as

$$\phi_p(z) = \frac{2.5}{h\nu_p A_p(z)} \exp(-2.6z) = \frac{10^{19}}{A_p(z)} \exp(-2.6z). \tag{4.1}$$

Here, ν_p is the pump light frequency and $A_p(z)$ is the area of the pump beam in the crystal. By using Equation (2.14), we calculate the steady-state population difference in the absence of radiation as

$$N_0 = \frac{6 \times 10^{15} \exp(-2.6z)/A_p(z)}{1 + 4.4 \times 10^{-5}/\exp(-2.6z)/A_p(z)}. \tag{4.2}$$

By integrating along the crystal length, this gives a small-signal gain coefficient of

$$\gamma_0 = \sigma \int_0^1 N_0(z) dz = 0.48. \tag{4.3}$$

In the calculation of Equation (4.3) the pump beam area is taken as $1.1 \times 10^{-3}\,cm^2$ from the entrance of the crystal to 2 mm, $1.2 \times 10^{-3}\,cm^2$ from 2 mm to 4 mm, $1.3 \times 10^{-3}\,cm^2$ from 4 mm to 6 mm, $1.4 \times 10^{-3}\,cm^2$ from 6 mm to 8 mm, and $1.6 \times 10^{-3}\,cm^2$ from 8 mm to 10 mm. This value for γ_0 is larger than those we measured for the lasers with -10 and -50 cm input couplers, 0.135 and 0.11 respectively. By using useless loss coefficients found for these lasers (0.05 and 0.02), we can calculate the output powers with the help of Equations (2.28) and (2.32). These are 1.1 W for the laser with -10 cm input coupler and 1.4 W for the laser with -50 cm input coupler. However, the measured output powers are 640 mW and 580 mW, respectively. This difference between the calculated and measured values is mainly caused from the calculations in which we do not consider the mode overlap between the pump and laser beams.

There are high efficiencies reported for the diode-end-pumped Nd:YAG lasers. The first paper with high efficiency figures came from Sipes [33] who showed 8% wall-plug efficiency and 37% optical conversion efficiency. In 1992, Yamaguchi [47] reported 10.1% wall-plug efficiency and 38% optical conversion efficiency. Later in 1993, Tidwell [36] reported 92 W multimode output power with 44% optical conversion efficiency.

Our relatively low wall-plug efficiencies are caused mainly from the uncoated optics we used. Another reason for low wall-plug efficiency is the non-optimal focusing of the pump beam. The latter is also the main cause of the low optical conversion efficiency.

4.4 Output beam profile

The output beam profiles of the lasers that we implemented show different characteristics. When the mode sizes are greater, we could obtain near Gaussian profiles (see Figure 4.20). This is the image of the beam from the laser with -50 cm input coupler, 93% output coupler, and 7.3 cm resonator length. However, when the curvatures of the input couplers and the resonator lengths decrease, the laser operates in higher order modes. Fundamental mode sizes become smaller for these lasers. Therefore, the pump beam size exceeds the fundamental mode size. Hence, some unused gain parts exist inside the gain medium. These regions initiates higher order modes, causing the laser to operate multi-transverse mode.

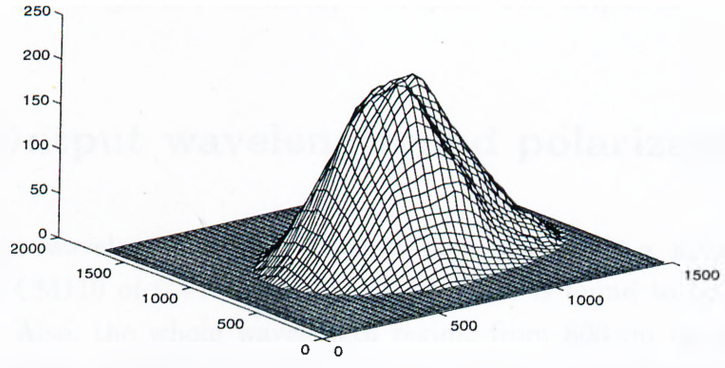

Figure 4.20: Beam profile of the laser, units are in micrometers.

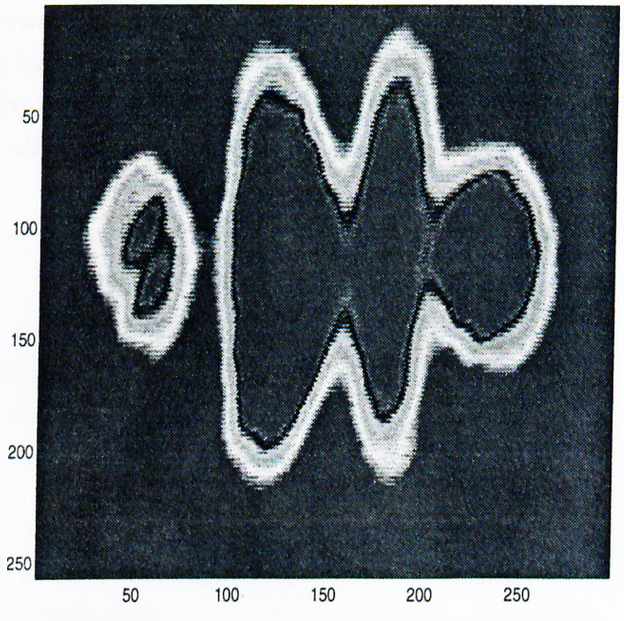

Figure 4.21: A higher order mode which occurs when the mirrors are slightly misaligned.

Forcing a multimode laser to lase in a single transverse mode can be done by inserting additional loss components to the higher order modes. This can be implemented by placing an aperture inside the laser to suppress higher order modes. We constructed a laser with an intracavity aperture and could run it only in TEM_{20} mode, not in TEM_{00} mode. However, the power decreased notably (from 600 mW to 110 mW). The reason for not achieving to operate the laser in TEM_{00} mode should be the large diameter of the aperture, so TEM_{20} mode was not suppressed.

Also, small misalignments of the mirrors cause the laser to operate in higher

order modes. Figure 4.21 is an example of a higher order mode. This laser has 6 cm resonator length and -10 cm input coupler. The output power is 380 mW.

4.5 Output wavelength and polarization

The output wavelength of our laser is measured with a monochromator (Digikröm CM110 of CVI Laser Corporation). It is found to be 1064 nm as expected. Also, the whole wavelength regime from 800 nm to 1600 nm was traced. However, none of the other possible lasing wavelengths were detected (i.e. 1300 nm and 946 nm).

Using a Brewster's angle cut Nd:YAG rod introduces a ratio of 500 between the round-trip losses of s and p-polarized waves in our laser. This is enough of a loss difference to force the laser to operate p-polarized. Therefore, our laser has a horizontally polarized output. The extinction ratio is measured to be 1:1700.

Chapter 5

RING RESONATOR DESIGN

We also implemented a laser using a ring resonator (see Figure 5.1).

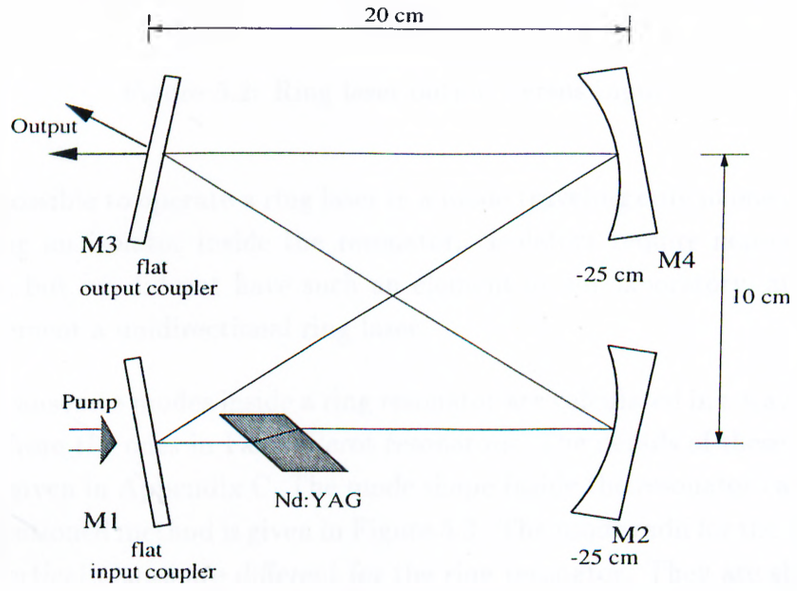

Figure 5.1: Ring laser geometry.

In this laser we observed two modes traveling in opposite directions. These modes were competing for the gain. Therefore, the output powers of these two modes were changing continuously, while the total power remained constant. The input output relation for this laser is given in Figure 5.2. The power shown in the figure is the sum of the powers of two modes. The data is taken with the 93% output coupler. No lasing is achieved with other output couplers. A maximum of 230 mW is obtained with this configuration and the threshold is 1.55 W. This relatively (with respect to Fabry-Perot lasers) low output is

typical for low gain lasers. As compared to Fabry-Perot lasers, we have higher losses (due to the higher number of mirrors) and lower gain (since the beam traverses the gain medium only once). The result is a decrease in the laser performance.

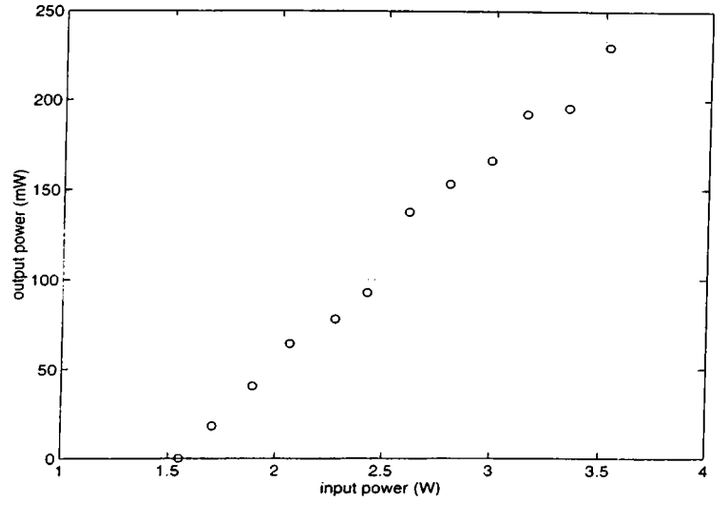

Figure 5.2: Ring laser output versus input.

It is possible to operate a ring laser in a mode traveling only in one direction by placing an isolator inside the resonator. Isolators require non-reciprocal elements, but we did not have such an element in our laboratory, and could not implement a unidirectional ring laser.

The transverse modes inside a ring resonator are calculated in a way slightly different from the ones in Fabry-Perot resonators. The details of these calculations are given in Appendix C. The mode shape inside the resonator calculated by the mentioned method is given in Figure 5.3. The mode radii for the horizontal and vertical planes are different for the ring resonator. They are shown by straight and dashed lines respectively in the figure. The mode radius is around 220 μm inside Nd:YAG which gives the maximum power for Fabry-Perot lasers.

The different mode radii for two perpendicular planes is caused from non-normal incidence angles at the mirrors. This also gives rise to astigmatism of the beam. To alleviate astigmatism, the incidence angles should be kept small. The incidence angles in our resonator was 13.6°.

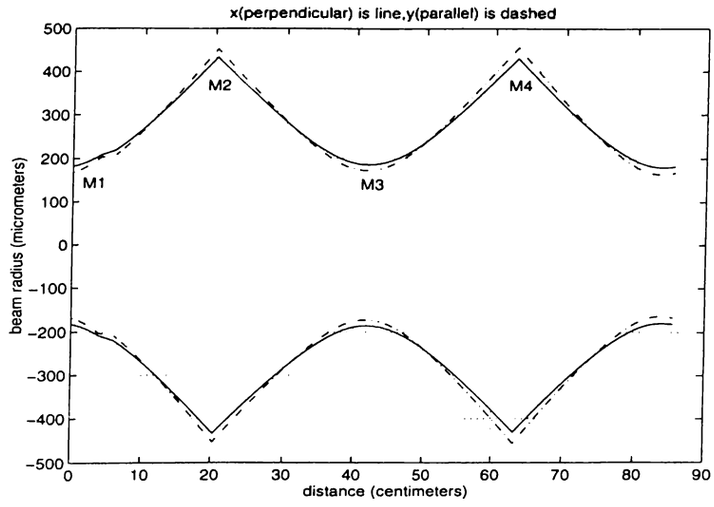

Figure 5.3: The mode radius inside the ring resonator. The straight and dashed lines correspond to beam radii at vertical and horizontal planes respectively.

Chapter 6

INTRACAVITY FREQUENCY DOUBLING

We achieved intracavity second harmonic generation by placing a Potassium Titanyl Phosphate (KTP) crystal inside the cavity. The crystal is cut at θ=90° and o=24° so that 1064 nm second harmonic generation is phase matched. The layout of the experiment is shown in the Figure 6.1.

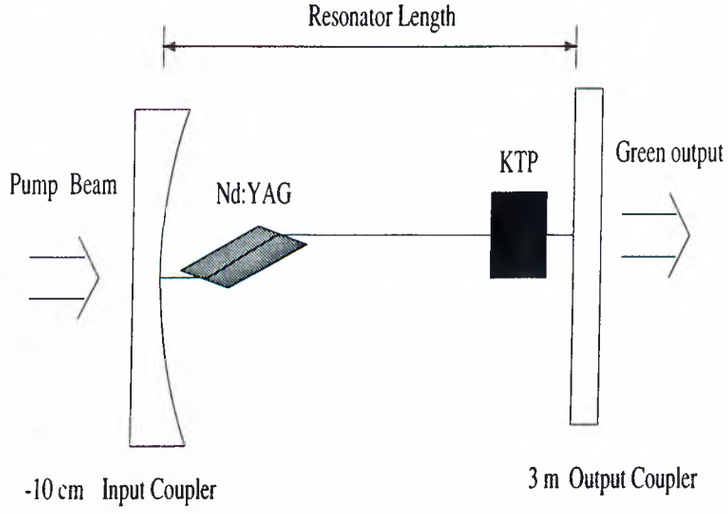

Figure 6.1: Intracavity second harmonic generation experiment.

Second harmonic generation is a nonlinear process which depends strongly on the intensity. To make the intensity high in the KTP, we put it where the mode radius is smallest (very close to the flat output coupler). We optimized the green output by changing the resonator length and the position of the KTP

crystal. Maximum second harmonic power was achieved using the -10 cm input coupler with the -3 m output coupler. This -3 m mirror has high transmittance at 532 nm and high reflectance at 1064 nm. The high reflectance at 1064 nm results in high intensities at 1064 nm in the resonator and high transmittance at 532 nm couples the green light out of the resonator.

This laser has output beams at 532 nm and 1064 nm. To measure the 532 nm portion, we employ a prism and separate these two frequencies. Results for the laser yielding maximum green power are given in Figure 6.2. 165 mW of maximum green power was obtained with this configuration. It has a nonlinear characteristic. The laser threshold is at 0.5 W.

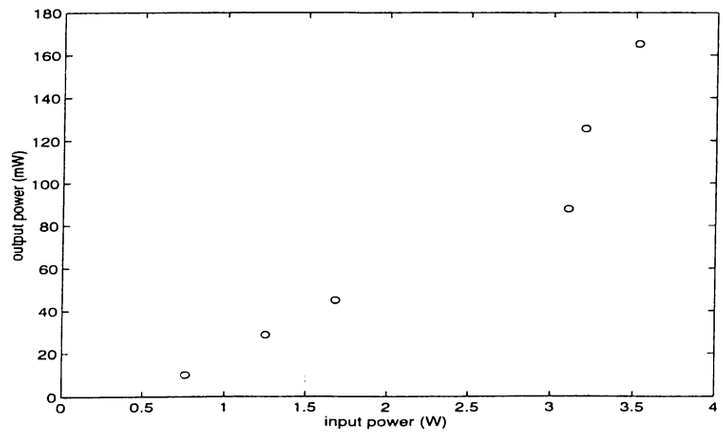

Figure 6.2: 532 nm power versus input power to Nd:YAG for the Fabry-Perot laser.

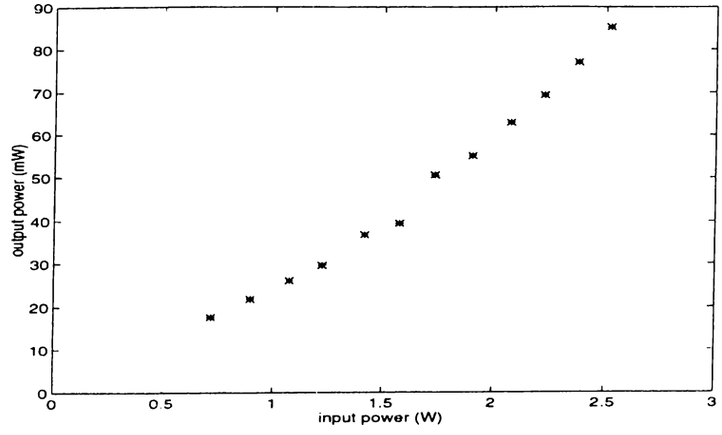

Figure 6.3: 532 nm power versus input power to Nd:YAG for the ring laser.

Intracavity second harmonic generation experiment was also implemented with the ring laser. A maximum of 85 mW of green power was obtained from this configuration (see Figure 6.3).

Chapter 7

CONCLUSIONS

In this thesis, we designed and built end-pumped Nd:YAG lasers. Lasing was achieved with Fabry-Perot and ring resonators. Also, second harmonic light was generated from these lasers.

The Nd:YAG crystal is noted to be a good choice for diode-pumped lasers. It lases with good efficiencies. However, when operated at high powers, thermal effects causes the output power to decrease. These effects should be minimized by better cooling the crystal.

It is seen that the Brewster's angle cut gain medium is a proper solution to get polarized laser outputs. It supplies necessary loss difference between orthogonal polarizations without using extra intracavity elements. However, the gain is reduced due to enlargement of the pump beam entering the Brewster's angle cut rod.

The TE cooler adjusts the temperature of the diode laser, and hence its wavelength. The output power of the laser can be maximized by varying the temperature of the diode laser. However, TE cooler current limits are exceeded when operating at full power at low temperatures. This limits the achievable diode laser wavelength range.

The pump beam spot size is observed to be a very important factor for laser performance. Non-Gaussian complex characteristics of the diode light at the plane parallel to the junction prohibited small spot sizes. This put a stringent limit on the gain of our laser and also caused multi transverse mode output beams in lasers with small mode radii. Therefore, we can conclude that production of high power diode lasers with Gaussian beams at both planes

would immediately increase the power level and the beam quality of diode-end-pumped Nd:YAG lasers.

The relatively low wall-plug efficiencies of our lasers are caused mainly from the surface reflections of the optics used in the experiments. To increase these efficiencies, optics that are anti-reflection coated at the proper wavelength should be used.

Suppressing higher order transverse modes by using an aperture did not seem to be a feasible way of getting single transverse mode output, since this decreased the output power too much. Therefore, the solution of single mode operation should be searched in better matching the pump and fundamental laser modes. Focusing the pump beam in a smaller area than the laser mode area would give a laser operating at fundamental mode.

In the ring laser, unidirectional output can be obtained by employing an isolator. The lacking element to construct an isolator is the non-reciprocal material. The Nd:YAG crystal can give the required non-reciprocity by using it with a magnet in an appropriate manner. By inserting a Q-switch in one of to its arms the laser can be run in pulsed mode. Also Fabry-Perot lasers can be run in pulsed mode by using a Q-switch.

In intracavity frequency doubling experiments, the output light is coupled from several mirrors in the resonator. To obtain proper output power at the second harmonic, mirrors properly coated at appropriate wavelengths are required.

Appendix A

GAUSSIAN BEAMS

Paraxial waves have wavefront normals making small angles with the direction of propagation [2]. The complex amplitude of such a wave can be given as

$$U(\mathbf{r}) = A(\mathbf{r}) \exp(-jkz) \tag{A.1}$$

where z is the propagation direction, $\mathbf{r}$ is the position vector and $A(\mathbf{r})$ is a slowly varying function of position. They must satisfy the paraxial Helmholtz equation

$$\nabla_T^2 A - j2k\frac{\partial A}{\partial z} = 0 \tag{A.2}$$

where $\nabla_T^2 = \partial^2/\partial x^2 + \partial^2/\partial y^2$ is the transverse Laplacian operator. An important solution of this equation is the Gaussian beam. The complex amplitude of a Gaussian beam is given by

$$U(\mathbf{r}) = \frac{A_1}{q(z)} \exp\left[-jk\frac{\rho^2}{2q(z)}\right] \exp(-jkz) \tag{A.3}$$

or in a more open form

$$U(\mathbf{r}) = A_0 \frac{W_0}{W(z)} \exp\left[-\frac{\rho^2}{W^2(z)}\right] \exp\left[-jkz - jk\frac{\rho^2}{2R(z)} + j\xi(z)\right] \tag{A.4}$$

and the intensity $I(\mathbf{r}) = |U(\mathbf{r})|^2$ can be written as

$$I(\rho, z) = |A_0|^2 \left[\frac{W_0}{W(z)}\right]^2 \exp\left[-\frac{2\rho^2}{W^2(z)}\right] \tag{A.5}$$

where in these equations

$$\rho^2 = x^2 + y^2 \tag{A.6}$$

$$q(z) = z + jz \tag{A.7}$$

$$\frac{1}{q(z)} = \frac{1}{R(z)} - j\frac{\lambda}{\pi W^2(z)} \tag{A.8}$$

$$W(z) = W_0 \left[1 + \left(\frac{z}{z_0}\right)^2\right]^{1/2} \tag{A.9}$$

$$R(z) = z\left[1 + \left(\frac{z_0}{z}\right)^2\right] \tag{A.10}$$

$$\xi(z) = \tan^{-1}\frac{z}{z_0} \tag{A.11}$$

$$W_0 = \left(\frac{\lambda z_0}{\pi}\right)^{1/2} \tag{A.12}$$

Equation (A.4) contains two parameters, A_0 and z_0. They are determined from the boundary conditions. All other parameters are related to Rayleigh range z_0 and the wavelength λ.

$W(z)$ is called the beam radius or the beam width. At the radial distance $\rho = W(z)$, the beam intensity drops by a factor $1/e^2$.The minimum value of $W(z)$ is at $z = 0$ and is called beam waist, W_0. The distance at which the beam radius equals $\sqrt{2}W_0$ is the Rayleigh range, z_0. Depth of focus is defined as $2z_0$. $\xi(z)$ is a phase retardation. $R(z)$ is the radius of curvature of the wavefront at position z.

Appendix B

RING LASER MODE CALCULATIONS

In ring resonators, there are two orthogonal planes of meridional symmetry instead of cylindrical symmetry which exists in linear (Fabry-Perot) resonators. The analysis of transverse modes in such a resonator can be done by extending the analysis of modes in linear resonators. Since there are two orthogonal planes, the wave equation can be uncoupled for these two planes. The solutions have the form

$$U(\mathbf{r}) = \frac{A_1}{\sqrt{q_x(z)q_y(z)}} \exp\left[-jk\frac{x^2}{2q_x(z)}\right] \exp\left[-jk\frac{y^2}{2q_y(z)}\right] \exp(-jkz). \quad \text{(B.1)}$$

This is an astigmatic (if $q_x \neq q_y$) Gaussian beam. It has different mode radii and curvatures in x and y planes.

To find the transverse modes in a ring resonator, one has to multiply the $ABCD$ matrices of the corresponding elements in the resonator in true order. The $ABCD$ matrix of the free space propagation is the same for x and y planes as expected

$$\begin{pmatrix} 1 & d \\ 0 & 1 \end{pmatrix}$$

It is well known that a concave mirror used at oblique incidence focuses horizontal ray bundles at a location different from that of vertical bundles [48, 49]. This is reflected in two different effective focal lengths, f_x and f_y (x plane horizontal, y plane vertical assumed)

$$f_x = R\cos\theta \quad \text{(B.2)}$$

$$f_y = R/\cos\theta \tag{B.3}$$

where θ is the angle of incidence and R is the radius of curvature of the mirror. Therefore, mirror matrices for x and y planes become, respectively

$$\begin{pmatrix} 1 & 0 \\ 2/R\cos\theta & 1 \end{pmatrix}$$

$$\begin{pmatrix} 1 & 0 \\ 2\cos\theta/R & 1 \end{pmatrix}$$

By multiplying these matrices in the proper order according to ring geometry, $ABCD$ matrices of the resonator is obtained for two planes

$$M_{x,y} = \begin{pmatrix} A_{x,y} & B_{x,y} \\ C_{x,y} & D_{x,y} \end{pmatrix}$$

Finding the resonator modes then becomes the search for the eigenvalues ($e_{x,y}$) of these 2x2 matrices because $q_{x,y}$ determining the mode characteristics is related the eigenvalues by the relation

$$q_{x,y} = (e_{x,y} - D_{x,y})/C_{x,y}. \tag{B.4}$$

The mode radius and the radius of curvature are depended to q values as

$$W_{x,y}^2 = \frac{-1}{\mathrm{Re}(ik/2q_{x,y})} \tag{B.5}$$

$$\frac{1}{R_{x,y}} = \mathrm{Re}\left(\frac{1}{q_{x,y}}\right). \tag{B.6}$$

A 2x2 matrix has two eigenvalues ϵ_1 and ϵ_2=$1/\epsilon_1$. If the eigenvalues are real, then the resonator is unstable. If the eigenvalues are complex, then ϵ_1=ϵ_2^* and it is found that one of these solutions has a negative value for $W_{x,y}^2$ and must be rejected as unphysical. The remaining solution gives the mode in the plane which it belongs. The combination of solutions in two planes shows that the resonator is stable (the eigenvalues are complex in both planes), unstable in both planes (both eigenvalues are real) or unstable in one direction but not in the other which means again unstability.

Appendix C

SPECIFICATIONS OF SDL-2382-P1 DIODE LASER

CW output power (W)	4.0
Differential quantum efficiency (%)	70
Slope efficiency (W/A)	1.06
Total conversion efficiency (%)	30
Emitting dimensions W X H (μm)	500 x 1.0
Beam divergence $\theta_{\perp}$, $\theta_{//}$ (deg FWHM)	34, 12
Threshold current (A)	1.97
I at 4.0 W (A)	5.76
V at 4.0 W (V)	1.89
Series resistance (Ω)	0.056
Recommended case temperature (°C)	-20 to 30
Spectral width (nm FWHM)	2.0
Temperature coeff. of wavelength (nm/°C)	0.27-0.3
Temperature coeff. of op. current (% per °C)	1.0
Wavelength range (nm)	797-815

Absolute Maximum Ratings

CW output power (W)	4.2
Reverse voltage (V)	3
Case operating temperature (°C)	-20 to 50
Storage temperature range (°C)	-55 to 60

Monitor Photodiode

Sensitivity (μA/mW)	:	0.3 to 10
Capacitance (pf)	:	6
Breakdown voltage (V)	:	25
Operating voltage (V)	:	10

Thermoelectric Cooler

Max. drive current (A)	:	3.5
Max. drive voltage (V)	:	8.0
Thermistor R @ 25°C (kΩ)	:	10

P1 HIGH HEAT LOAD (>1 W) WINDOW PACKAGE

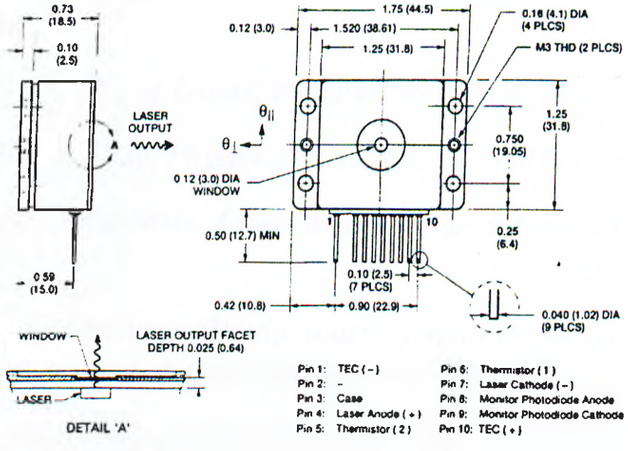

Figure C.1: Diode package specifications.

REFERENCES

[1] T. H. Maiman, *Nature*, vol. 187, p. 493, 1960.

[2] B. E. A. Saleh, M. C. Teich, *Fundamentals of Photonics*, John Wiley & Sons Inc., New York, 1991.

[3] A. E. Siegman, *Lasers*, University Science Books, Mill Valley, California, 1986.

[4] H. Kogelnik, T. Li, "Laser beams and resonators", *Applied Optics*, vol. 5, p. 1550, 1966.

[5] O. Svelto, *Principles of Lasers*, Plenum Press, New York, 1982.

[6] D. Findlay, R. A. Clay, *Physics Letters*, vol. 20, p.277, 1966.

[7] W. Koechner, *Solid-State Laser Engineering*, Springer Verlag, Berlin, 1991.

[8] T. Y. Fan, A. Sanchez. "Pump source requirements for end-pumped lasers", *IEEE Journal of Quantum Electronics*, vol. 26, p. 311, 1990.

[9] T. Y. Fan, "Modelling and CW operation of a quasi three-level 946 nm Nd:YAG laser" , *IEEE Journal of Quantum Electronics*, vol. QE-23, p. 605, 1987.

[10] W. P. Risk, "Modelling of longitudinally pumped solid-state lasers exhibiting reabsorption losses", *Journal of the Optical Society of America B*, vol. 5, p. 1412, 1988.

[11] L. W. Casperson, "Laser power calculations: sources of error", *Applied Optics*, vol. 19, p. 424, 1980.

[12] D. G. Hall, R. J. Smith, R. R. Rice, "Pump-size effects in Nd:YAG lasers", *Applied Optics*, vol. 19, p. 3041, 1980.

[13] D. G. Hall, "Optimum mode size criterion for low-gain lasers", *Applied Optics*, vol. 20, p. 1579, 1981.

[14] A. J. Alfrey, "Modeling of longitudinally pumped cw Ti:saphire laser oscillators", *IEEE Journal of Quantum Electronics*, vol. 25, p. 760, 1989.

[15] I. H. Hwang, W. E. Meador, "An analytical model for longitudinally pumped continuous-wave laser", *Journal of Applied Physics*, vol. 72, p. 2556, 1992.

[16] C. Pfitsiner, P. Albers, H. P. Weber, "Influence of spatial mode matching in end-pumped solid state lasers", *Applied Physics B*, vol. 54, p. 83, 1992.

[17] N. Bloembergen, *Nonlinear Optics*, Addison-Wesley, Reedwood City, California, 1965.

[18] A. L. Schawlow, C. H. Townes, "Infrared and optical masers", *Physical Review*, vol. 112, p. 1940, 1958.

[19] R. Newman, "Excitation of the Nd^{3+} fluorescence in $CaWO_4$ by recombination radiation in GaAs", *Journal of Applied Physics*, vol. 34, p. 437, 1963.

[20] R. J. Keyes, T. M. Quist, "Injection luminescent pumping of CaF_2:U^{3+} with GaAs diode lasers", *Applied Physics Letters*, vol. 4, p. 50, 1974.

[21] R. N. Hall, G. E. Fenner, J. D. Kingsley, T. J. Soltys, R. O. Carlson, "Coherent light emission from GaAs junctions", *Physical Review Letters*, vol. 9, p. 366, 1962.

[22] M. Ross, "YAG laser operation by semiconductor laser pumping", *Proceedings of IEEE*, vol. 56, p. 196, 1968.

[23] R. B. Allen, S. J. Scalise, "Continuous operation of a YAlG:Nd laser by injection luminescent pumping", *Applied Physics Letters*, vol. 14, p. 188, 1969.

[24] F. W. Ostermayer, "$GaAs_{1-x}P_x$ diode pumped YAG:Nd lasers", *Applied Physics Letters*, vol. 18, p. 93, 1971.

[25] F. W. Ostermayer, R. B. Allen, E. G. Dierschke, "Room temperature cw operation of a $GaAs_{1-x}P_x$ diode pumped YAG:Nd laser", *Applied Physics Letters*, vol. 19, p. 289, 1971.

[26] H. G. Danielmayer, F. W. Ostermayer, "Diode-pump-modulated Nd:YAG laser", *Journal of Applied Physics*, vol. 43, p. 2911, 1972.

[27] L. C. Conant, "GaAs laser diode pumped Nd:YAG laser", *Applied Optics*, vol. 13, p. 2457, 1974.

[28] L. J. Rosenkrantz, "GaAs diode-pumped Nd:YAG laser", *Journal of Applied Physics*, vol. 43, p. 4603, 1973.

[29] R. B. Chesler, D. A. Draegert, "Miniature diode-pumped Nd:YAlG lasers", *Applied Physics Letters*, vol. 23, p. 235, 1973.

[30] D. A. Draegert, "Single-diode end-pumped Nd:YAG laser", *IEEE Journal of Quantum Electronics*, vol. QE-9, p. 1146, 1973.

[31] K. Washio, K. Iwamoto, K. Inoue, I. Hino, S. Matsumoto, F. Saito, "Room-temperature cw operation of an efficient miniaturized Nd:YAG laser end-pumped by a superluminescent diode", *Applied Physics Letters*, vol. 29, p. 720, 1976.

[32] F. W. Ostermayer, "LED end-pumped Nd:YAG lasers", *IEEE Journal of Quantum Electronics*, vol. QE-13, p. 1, 1977.

[33] D. L. Sipes, "Highly efficient neodymium: yttrium aluminum garnet laser end pumped by a semiconductor laser array", *Applied Physics Letters*, vol. 47, p. 74, 1985.

[34] J. Berger, D. F. Welch, D. R. Scifres, W. Streifer, P. Cross, "High power, high efficient neodymium:yttrium aluminum garnet laser end pumped by a laser diode array", *Applied Physics Letters*, vol. 51, p. 1212, 1987.

[35] D. C. Shannon, R. W. Wallace, "High power Nd:YAG laser end pumped by a cw, 10-W laser-diode bar", *Optics Letters*, vol. 16, p. 318, 1991.

[36] S. C. Tidwell, J. F. Seamans, M. S. Bowers, "Highly efficient 60-W TEM_{00} cw diode-end-pumped Nd:YAG laser", *Optics Letters*, vol. 18, p. 116, 1993.

[37] T. Baer, M. S. Keirstead, "Intracavity frequency doubling of a Nd:YAG laser pumped by a laser diode array", in *Postdeadline Papers , Conf. Lasers Electro-Opt.*. paper ThZZ1, Opt. Soc. Amer., Washington DC, 1985.

[38] R. Burnham, A. D. Hays, "High-power diode-array-pumped frequency doubled CW Nd:YAG laser", *Optics Letters*, vol. 14, p. 27, 1989.

[39] D. W. Anthon, D. L. Sipes, T. J. Pier, M. R. Ressl, "Intracavity doubling of CW diode-pumped Nd:YAG lasers with KTP", *IEEE Journal of Quantum Electronics*, vol. 28, p. 1148, 1992.

[40] H. Nagai, M. Mume, I. Ohta, H. Shimizu, M. Kazumura, "Low noise operation of a diode-pumped intracavity-doubled Nd:YAG laser using a

Brewster plate", *IEEE Journal of Quantum Electronics*, vol. 28. p. 622, 1992.

[41] A. R. Clobes, M. J. Brienza, "Single-frequency travelling-wave Nd:YAG laser", *Applied Physics Letters*, vol. 21, p. 265, 1972.

[42] T. J. Kane, R. L. Byer, "Monolithic, unidirectional single mode Nd:YAG ring laser", *Optics Letters*, vol. 10. p. 65, 1985.

[43] W. R. Trutna, D. K. Donald, M. Nazarathy, "Unidirectional diode-laser-pumped Nd:YAG ring laser with a small magnetic field", *Optics Letters*, vol. 12, p. 248, 1987.

[44] J. Harrison, A. Finch, P. F. Moulton, "Rapidly tunable, single frequency, diode-pumped Nd:YAG laser", in *Digest of topical Meeting on Advanced Solid State Lasers*, paper MF3, Opt. Soc. Amer., Washington, DC, 1991.

[45] R. Scheps, J. Myers, "Single frequency Nd:YAG ring laser pumped by laser diodes", *IEEE Journal of Quantum Electronics*, vol. 26, p. 413, 1990.

[46] R. Scheps, J. Myers, "Scalable single-frequency diode-pumped ring laser", *Applied Optics*, vol. 31, p. 1221, 1992.

[47] S. Yamaguchi, H. Imai, "Efficient Nd:YAG laser end-pumped by a 1 cm aperture laser-diode bar with a GRIN lens array coupling", *IEEE Journal of Quantum Electronics*, vol. 28, p. 1101, 1992.

[48] X. Wang, G. Hu, Y. Li, J. Yao, "Numerical analysis of beam parameters and stability regions in a folded or ring cavity", *Journal of the Optical Society of America*, vol. 11, p. 2265, 1994.

[49] F. A. Jenkins, H. E. White, *Fundamentals of Optics*, McGraw-Hill, Auckland, 1985.